FREQUENCY-DEPENDENT AMPLITUDE ANALYSIS FOR OIL DETECTION WITHIN THE MIDDLE JURASSIC SEDIMENTARY ROCKS IN THE SOUTHERN PART OF WESTERN SIBERIA

A Thesis

Presented to

the Faculty of the Department of Earth and Atmospheric Sciences

University of Houston

In Partial Fulfillment

Of the Requirements for the Degree

Master of Science

By

Irina Privalova

May 2015

FREQUENCY-DEPENDENT AMPLITUDE ANALYSIS FOR OIL DETECTION WITHIN THE MIDDLE JURASSIC SEDIMENTARY ROCKS IN THE SOUTHERN PART OF WESTERN SIBERIA

Irina Privalova

APPROVED:

Dr. John Castagna, Chairman

Dr. Gennady Goloshubin

Dr. Evgeny Chesnokov

Dr. Haitao Ren

Dean, College of Natural Sciences and Mathematics

ACKNOWLEDGEMENTS

I would like to express my deepest appreciation to my thesis advisor, Dr. Gennady Goloshubin, for his invaluable assistance, support, and guidance. My graduate study and this thesis would not have been possible without his supervision and constant help.

A special gratitude I give to the members of my committee, Dr. John Castagna, Dr. Evgeny Chesnokov, and Dr. Haitao Ren, for all their comments, time and efforts. I would like to thank Dr. Fred Hilterman for his useful remarks and engagement through the learning process of this master thesis.

I would like to thank the West-Siberian Research Institute of Geology and Geophysics, and especially Yuriy Tcimbaluk, for the data, encouragement, and continuous support during my graduate study. Also I want to thank Pavel Rusakov for his help and strong collaboration during my study.

I am deeply thankful to my family, my father Vasiliy, my sister Kseniya, and my husband Artem, for always believing in me and for their unconditional love, understanding, support, courage, and help during these two years.

I dedicate this in loving memory of my mother, Olga, who always supported me, believed in me, and taught me to never give up.

FREQUENCY-DEPENDENT AMPLITUDE ANALYSIS FOR OIL DETECTION WITHIN THE MIDDLE JURASSIC SEDIMENTARY ROCKS IN THE SOUTHERN PART OF WESTERN SIBERIA

An Abstract of a Thesis

Presented to

the Faculty of the Department of Earth and Atmospheric Sciences

University of Houston

In Partial Fulfillment

Of the Requirements for the Degree

Master of Science

By

Irina Privalova

May 2015

ABSTRACT

The Middle Jurassic (Ju_{3-4}) sandstone reservoirs are characterized by the presence of non-structural types of traps, which are usually located on the slopes of anticlines and have stratigraphic, tectonic, and lithological barriers. Therefore, the structural element is not a determinative factor for identification of the hydrocarbon deposits within the Ju_{3-4} formation. In order to detect hydrocarbons, amplitude variations versus offset and frequency were analyzed.

The amplitude of the reflected wave from the Ju_{3-4} formation is affected by an interference with the strong reflected wave from the Bazhenovskaya (B) formation. Frequency-dependent amplitude analysis shows that at low frequencies (10 Hz) the effect of the strong reflected wave of the B formation is almost suppressed. Moreover, at this frequency the amplitude anomalies of the target reflected wave (Ju_{3-4}) were detected near the oil wells. This phenomenon allowed consideration of the low-frequency (LF) as a direct hydrocarbon indicator.

However, the modelling shows that the variation of the reservoir thickness has a remarkable influence on the reflected wave from the reservoir at low frequencies. In order to consider the effect of the thickness variation, the additive model of the influence of thickness variations on the LF attribute was developed and applied. As a result of the thickness compensation, a better correlation between the LF attribute anomalies and pure oil wells was obtained.

The LF attribute only allows for a qualitative separation of oil-saturated zones from water-saturated zones. The correlation between the LF attribute and formation resistivity was investigated in order to create quantitative criteria that could distinguish

the oil-saturated zones from water-saturated zones. Finally, the resistivity map was constructed. The map shows sufficient correlation with the oil saturation obtained from the well drilling.

TABLE OF CONTENTS

LIST OF FIGURES

CHAPTER ONE

INTRODUCTION

1.1 Motivation and objectives

The West Siberian oil-and-gas province is still one of the most prospective areas for searching of hydrocarbon deposits. Major oil-and-gas fields in this territory were opened relying on the structural factor. Since the largest hydrocarbon deposits have already been discovered, seismic interpretation studies have begun focusing on the oil and gas traps with a smaller size and structural complexity.

In the southern regions of Western Siberia, the most prospective targets for oil and gas are in Jurassic sedimentary rocks. The Jurassic formations are characterized by high heterogeneity. They are often located on the slopes of the structures and usually have lithological, stratigraphic, and tectonic barriers. Therefore, the traditional method of detecting oil and gas zones on the basis of the structural factor is ineffective in this case. The reservoirs in Jurassic strata are usually dense, low-porous, and low-permeable sandstones. However, the oil-and-gas potential of Jurassic deposits is still high. It accounts for more than 40% of the total oil-and-gas reserves in Western Siberia. Hence, it is critical to be able to predict the hydrocarbon saturation of the reservoirs considering that the structural element of a prospect is not a key factor in the detection of hydrocarbon deposits. In this regard, it makes sense to apply the combination of various seismic interpretation techniques with the support of information from the already drilled wells in order to detect hydrocarbon saturation within the area.

Amplitude analysis over the years has proved itself as a successful method for the determination of oil and gas fields. For example, frequency-dependent (FD) analysis of the amplitudes considers seismic reflections at different frequencies (Castagna et al., 2003; Goloshubin et al., 2002, 2006); while amplitude versus offset (AVO) analysis is based on the change of the amplitude of the reflections from the hydrocarbon-saturated reservoir with offset (Hilterman, 2001). In this work these two techniques have been used in order to analyze and determine the method that could be useful in the detection of oil deposits within the Middle Jurassic sediments. Also, well log data were involved in the analysis, and the formation resistivity was used as a supportive parameter for the quantitative separation of oil-saturated zones from water-saturated zones

Analysis was carried out on an area of one of the fields located in the southern Tyumen region (Figure 1.1) in the interval of major hydrocarbon reservoirs within Ju_3 and Ju_4 (Ju_{3-4}) formations at the top of the Middle Jurassic. The area is situated in the oil-prone Togur-Tyumen Total Petroleum System, where gas reserves are insignificant (Ulmishek, 2003) (Figure 1.2). This area has a three-dimensional seismic survey of about 500 km^2, where 15 wells were drilled. As a result of the Ju_{3-4} formations testing there is a flow of oil in four wells, water in five wells, and oil with water in six wells. 3D seismic data including gathers were used, and well logging materials and test results were involved in the analysis.

The main objectives of this work, in order to detect the oil-saturated zones within the Middle Jurassic sedimentary rocks in the southern part of Western Siberia, are: to analyze the amplitude behavior versus offset, to carry out the frequency-dependent amplitude analysis, to form the rule for the direct hydrocarbon detection that will be applicable in the territory, and to get the resulting prognostic map of oil saturation.

Figure 1.1 Satellite map showing the location of the study area (red rectangle)

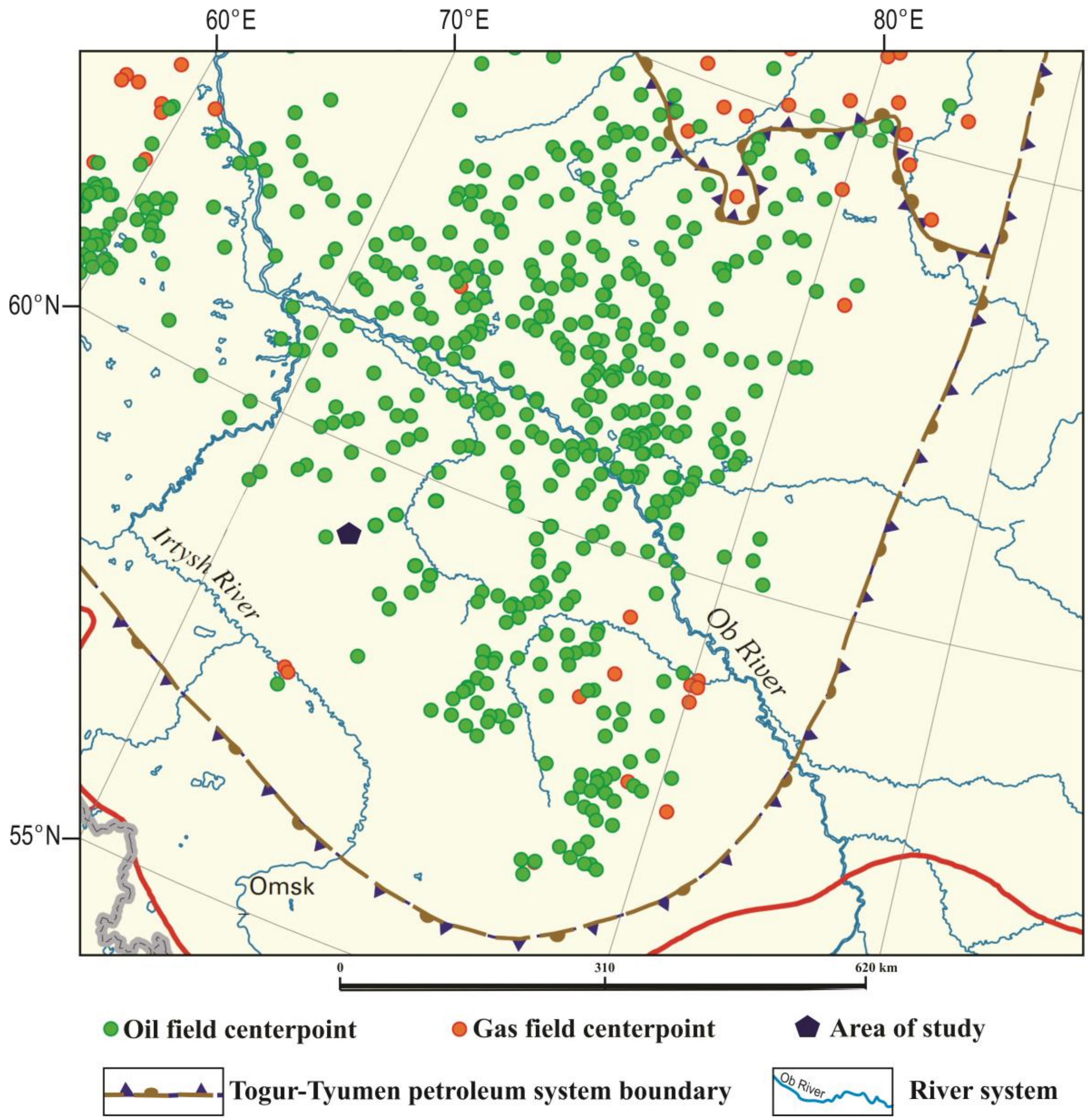

Figure 1.2 Hydrocarbon exploration wells in the Togur-Tyumen Total Petroleum System in the south of Western Siberia (modified from Ulmishek, 2003)

CHAPTER TWO

GEOLOGICAL AND GEOPHYSICAL OVERVIEW

2.1. Stratigraphy

Administratively, the working territory is located in the southern area of the Tyumen region in Western Siberia, Russia. The area is a swampy lake-alluvial plain. The terrain is divided by a well-developed erosional activity of rivers. The subject of detailed study is Jurassic sedimentary deposits and the petroleum potential of the West Siberian Plain that is associated with them. The Jurassic deposits occur throughout the described area, covering an angular unconformity, folded Paleozoic basement rocks, and volcanic-sedimentary Triassic rocks.

By litho-facies composition, the Jurassic section is subdivided into a number of formations and packs, a portion of which involves reflection of seismic horizons. Jurassic sediments accumulated in alluvial, proalluvial, swamp, and marsh environments, and in the upper part of the section sediments accumulated in coastal marine environments. The formation is represented by an alternation of gray-colored, sometimes brownish sandstone, siltstone, and compacted clay. Rocks are rich in plant detritus and debris timber. There are interlayers and lenses of carbonate rocks.

The source rock for the Jurassic is bituminous clays of the Bazhenovskaya formation. The Bazhenovskaya formation is a regional reference reflector for detailed seismic horizon’s correlation, and the main reflecting horizon according to seismic prospecting in Western Siberia. Bituminous siliceous rocks of the Bazhenovskaya formation are relatively thin in the context of the sedimentary cover of the West Siberian plate (up about 1%), but they are present over a wide area (more than 1 million km^2) (Ulmishek, 2003). The Bazhenovskaya formation is developed in all sections of the drilled wells in the observed area. Its thickness ranges from 35 to 45 m in this region. Upper parts of the Bazhenovskaya Formation directly overlie a weathering crust or eroded surface of pre-Jurassic complexes.

The Jurassic section is divided into three formations: Lower, Middle and Upper (Figure 2.1). This separation is based on a degree of predominance of clays or sandstones; at the same time the lithological composition of these stratigraphic units is almost absolutely uniform. This work is mainly concentrated on the hydrocarbon potential of the Middle Jurassic formation.

High heterogeneity of the geological section is inherent to the Middle Jurassic formations. Traps are usually structural, stratigraphic, or a combination of the two (Ulmishek, 2003). The deposits of the Middle Jurassic period are mostly siltstones or claystones. Three sandstones layers (Ju_2, Ju_3 and Ju_4) are found in the geological section. The Ju_2 formation is strongly sealed off, while the Ju_{3-4} formation is characterized by the absence of the stable clay seals. A presence of oil is related mainly with the Ju_{3-4} formation which lies beneath the Upper Jurassic regional clay cap rock.

The Ju_{3-4} formation was formed during the gradual onset of the marine basin in the Middle Jurassic lake-alluvial plain. It was accompanied by the formation of shallow deltaic zones, i.e., lake-sea water bodies, where sandbars sediments were accumulated. This is caused by increased sand content and improved sorting of clastic rocks. Here the sandstone to shale ratio is higher and the content of carbonaceous layers is lower than in other parts of the Middle Jurassic. Overlying clay deposits are confining beds for the Ju_{3-4} formation's reservoirs; they formed upon the occurrence of the Callovian marine transgression (Gurari et al., 2005). Due to the structural features of the Middle Jurassic most oil deposits discovered in the considered territory are related to the Ju_{3-4} stratigraphic level (Shymanskiy et al., 2004). According to the borehole and seismic information, sandstone reservoirs within the Ju_3 and Ju_4 formations have a discrete distribution and a complex irregular shape. They are mostly associated with non-structural types of traps. Hence, the structural factor is not determined in the identification of hydrocarbon deposits within the Ju_{3-4} formation.

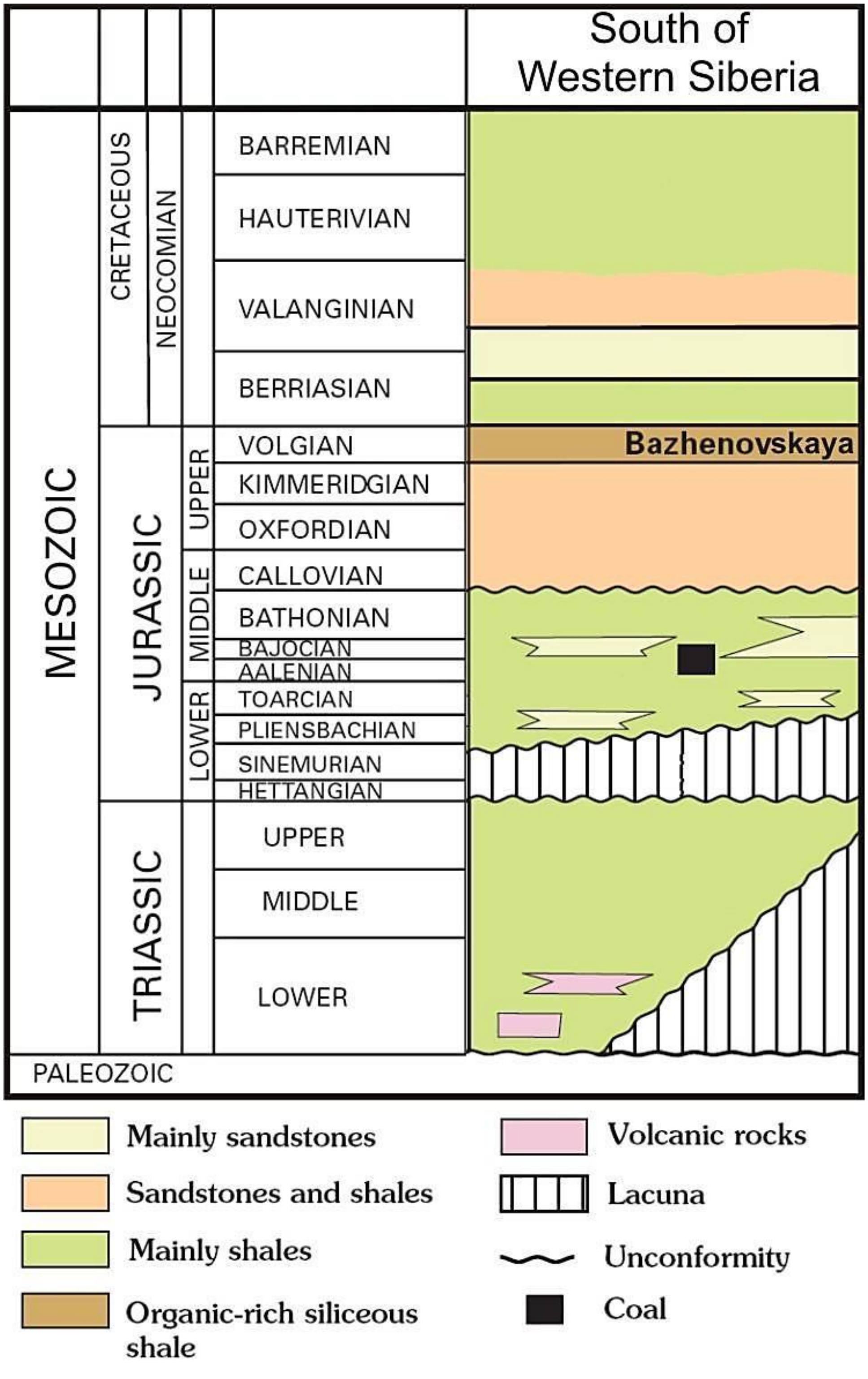

Figure 2.1 Section of Mesozoic rocks of the south of West Siberian basin (modified from Ulmishek, 2003)

2.2 Tectonics

Tectonics is one of the decisive factors in the formation of hydrocarbon traps. Hence, it is important to consider the main features of the tectonics of the study area. The considered territory of the south Tyumen region is located in the south-western part of the West Siberian geosyncline at the junction of a number of sub-regional, superorder, first-order, and second-order tectonic structures developed in the central areas. According to this classification, sub-regional structures are represented by extra-large and lengthy structures, such as mega terraces. Regional hemisynclines, synclines, and anticlines are referred to as superorder structures. First-order (depressions, swells, etc.) and second-order (mega troughs, shafts, etc.) structures are parts of superorder structures, and are separated into orders according to size.

Heterogeneity and block structure of the folded basement predetermined wide development of disjunctive dislocations of varying length and amplitude in the sedimentary cover. Development of elongated structures (megashafts, shafts, deflections, etc.) predominantly occurs. Flexures are widely developed in the cover.

Tectonically the studied area is a part of one of the largest sub-regional tectonic structures of the inner tectonic region of the West Siberian geosyncline Central mega terrace. In its turn the Central mega terrace is represented by the Sredneirtyshskaya syncline and the Mansiiskaya hemisyncline in this area (Figure 2.2).

The Demyansko-Tebissky shafts belt stands out within the Sredneirtyshskaya syncline. It has an explicit northwest strike and separates the Mansiiskaya hemisyneclise from the Sredneirtyshskaya syncline on a significant part of the western territory. The largest element of this tectonic megaswells belt is the Demianskiy megaswell. Being located in the largest Sredneirtyshskaya syncline, it is significantly different from other similar structures of the West Siberian geosyneclise and stands out with a certain degree of conditionality at this stage of exploration maturity. The Demianskiy megaswell is complicated by a number of shafts and deflections of the western and northern spread. The Tamarginsky swell is the largest part of the Demianskiy megaswell and is complicated by dome-shaped raisings. From the west and southwest the Demianskiy megaswell is limited by structures of Khanty-Mansiisk depression.

Within the Mansiskaya hemisyneclise, the Khanty-Mansiisk Depression and Muromsevskiy large trough are allocated. They consist of second-order structures: the Demyansko-Salymskaya mega trough and Kazim-Nizhnedemyanskaya mega depression. The major interest is dedicated to the Khanty-Mansiisk depression which occupies a large part of the considered territory.

The area of study is located in the junction of the Khanty-Mansiisk depression and Pihtovoe large uplift. These two first-order structures are separated by a part of the Demyano-Tebissky shafts belt. Tectonic conditions are essential in order to understand the structural features of the considered area. The above-mentioned tectonic elements are set mainly in the area of depression, which makes them favorable for hydrocarbon accumulation and formation of petroleum deposits.
From the obtained tectonic information we can expect different tectono-stratigraphic zones within the study area.

This brief review clearly demonstrates that most of the described area has potential in structural and tectonic conditions for the search of hydrocarbon accumulation in the Jurassic sediments.

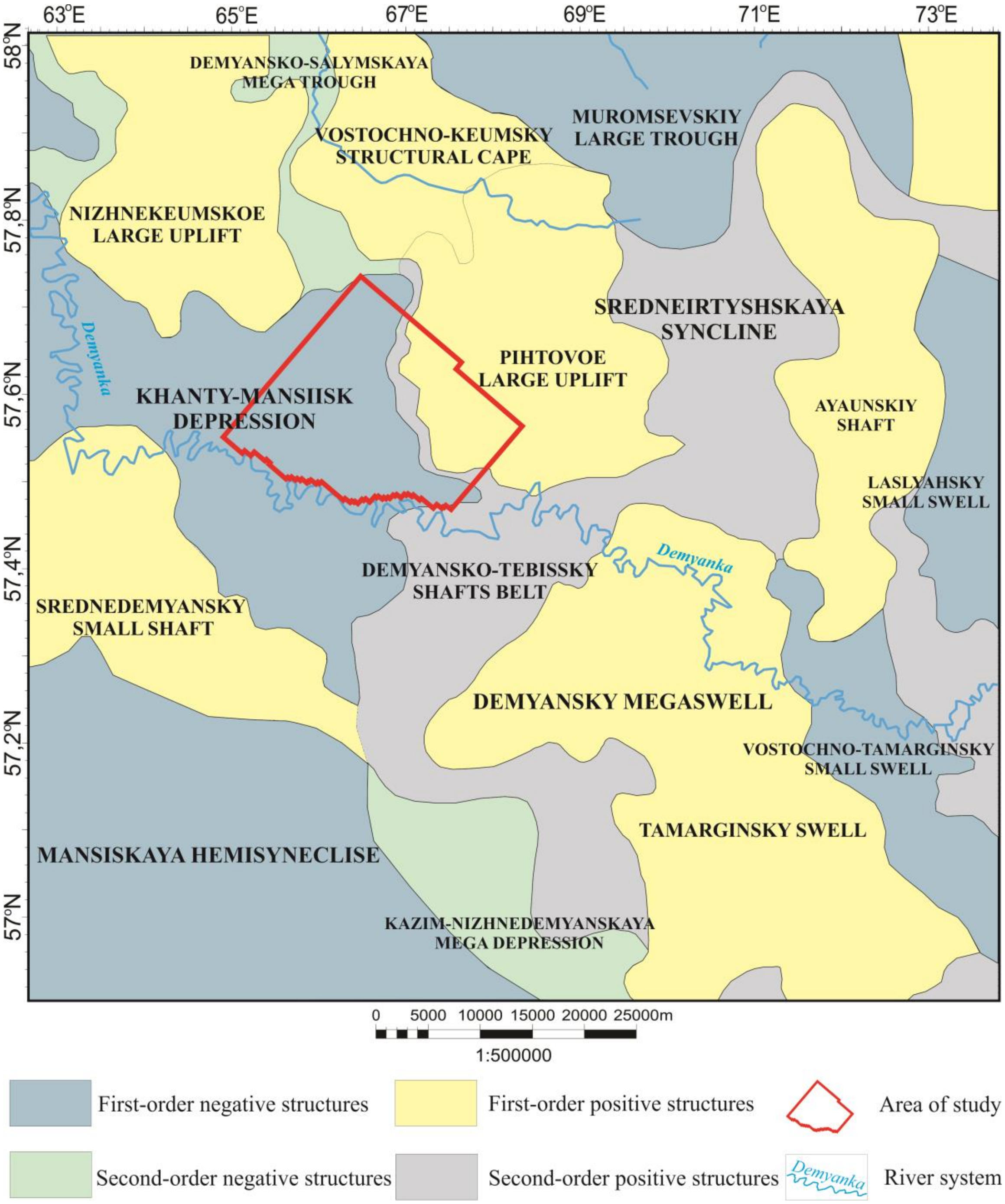

Figure 2.2 Tectonic map of the south Tyumen region in the southern part of Western Siberia of Mesozoic (modified from Bochkarev, 1977)

2.3 Seismic and log data

For the prediction of reservoirs' oil saturation within the study area, 3D seismic data were used. The survey area is 500 square kilometers (Figure 2.3). A seismic survey was made using a common depth point method. The observation system is orthogonal, where the source and receiver lines are perpendicular to each other. The distance between the sources is 100 m; the distance between the receivers is 50 m (Figure 2.4).

Fifteen wells were drilled at this territory. Logging studies were conducted in all wells. The standard complex consists of acoustic, gamma-gamma density, resistivity, spontaneous potential, and gamma logs. However, only six wells included the full complex within the Ju_{3-4} formation; the other wells were only partially logged. Figure 2.5 illustrates the well section of well #6 with the full complex of well logs.

Seismic data processing. The obtained seismograms were processed with the preservation of the amplitude and frequencies in the Geo Vector software system, CGG. It included the following procedures: a) preprocessing, which includes demultiplexing, reformatting data into SEG-Y format, editing seismic traces, setting up field geometry, correcting amplitude for the geometrical spreading, and applying priori statics; b) NMO-correction; c) sorting gathers to CMP format and muting; d) surface-consistent deconvolution and trace balancing; e) residual statics correction and velocity analysis; f) multiple suppression; g) pre-stack time Kirchhoff migration and stacking.

The result of processing is a timing seismic cube, which was subsequently used for interpretation. Quality of the processed data can be seen in crossline and inline sections (Figure 2.6, Figure 2.7). A clear wave pattern and good signal-to-noise ratio can be observed on the sections. Processing was made by the team from West-Siberian Research Institute of Geology and Geophysics

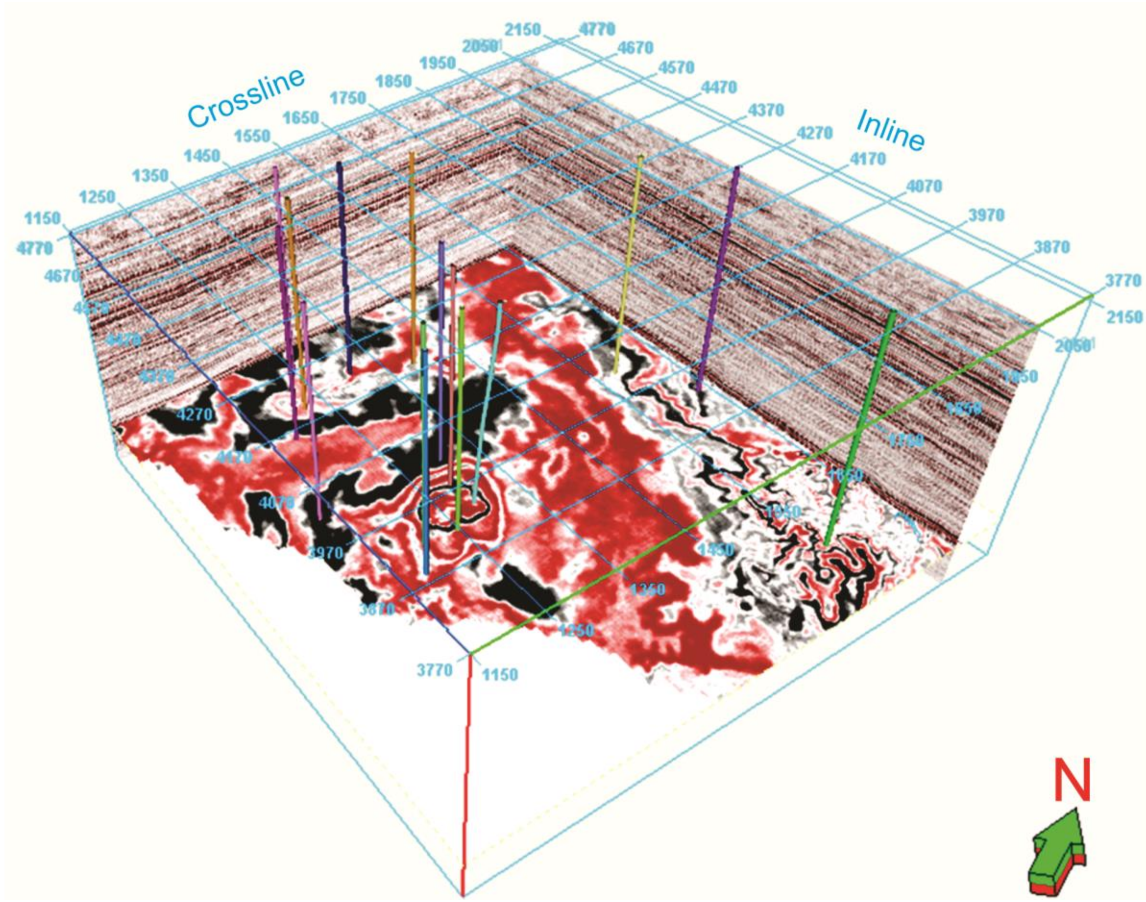

Figure 2.3 3D seismic volume with 15 drilled wells.

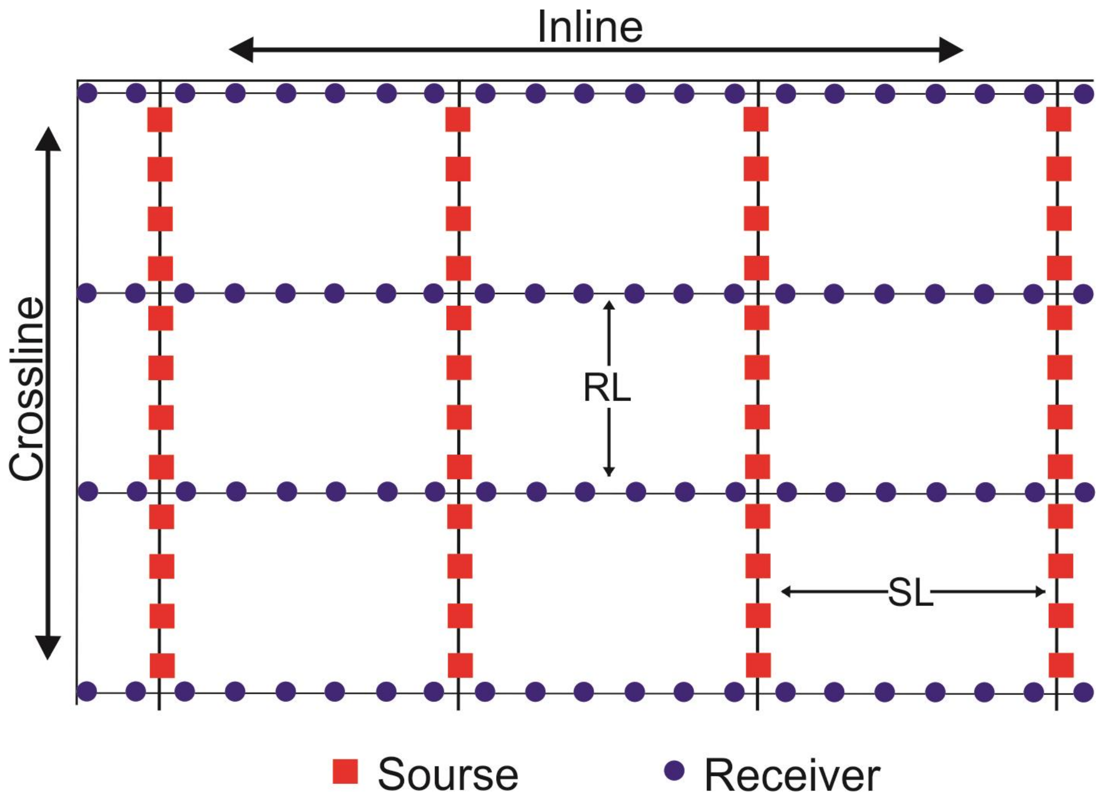

Figure 2.4 Orthogonal observation system

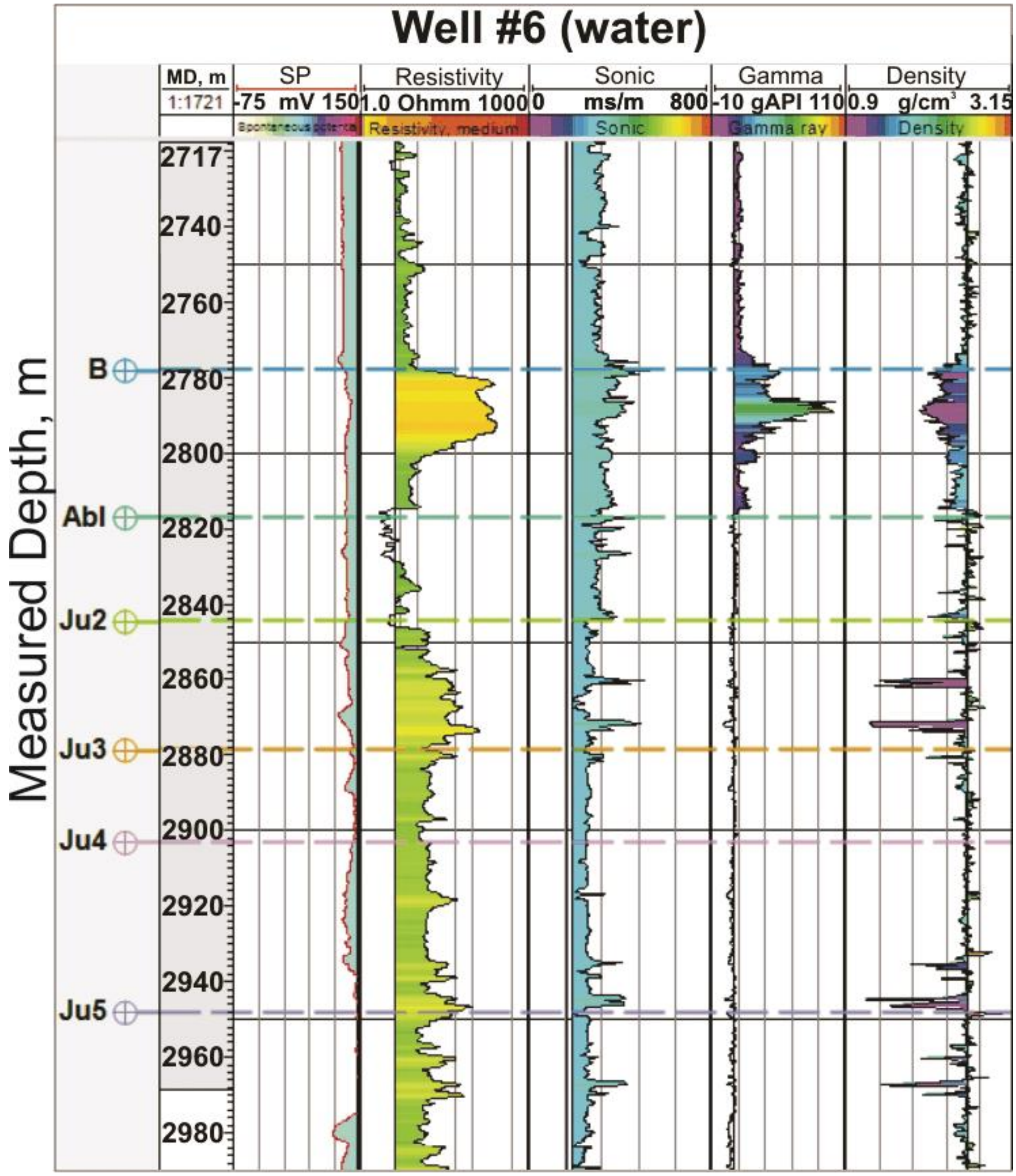

Figure 2.5 Complex of well-logging methods in the well #6 (water).

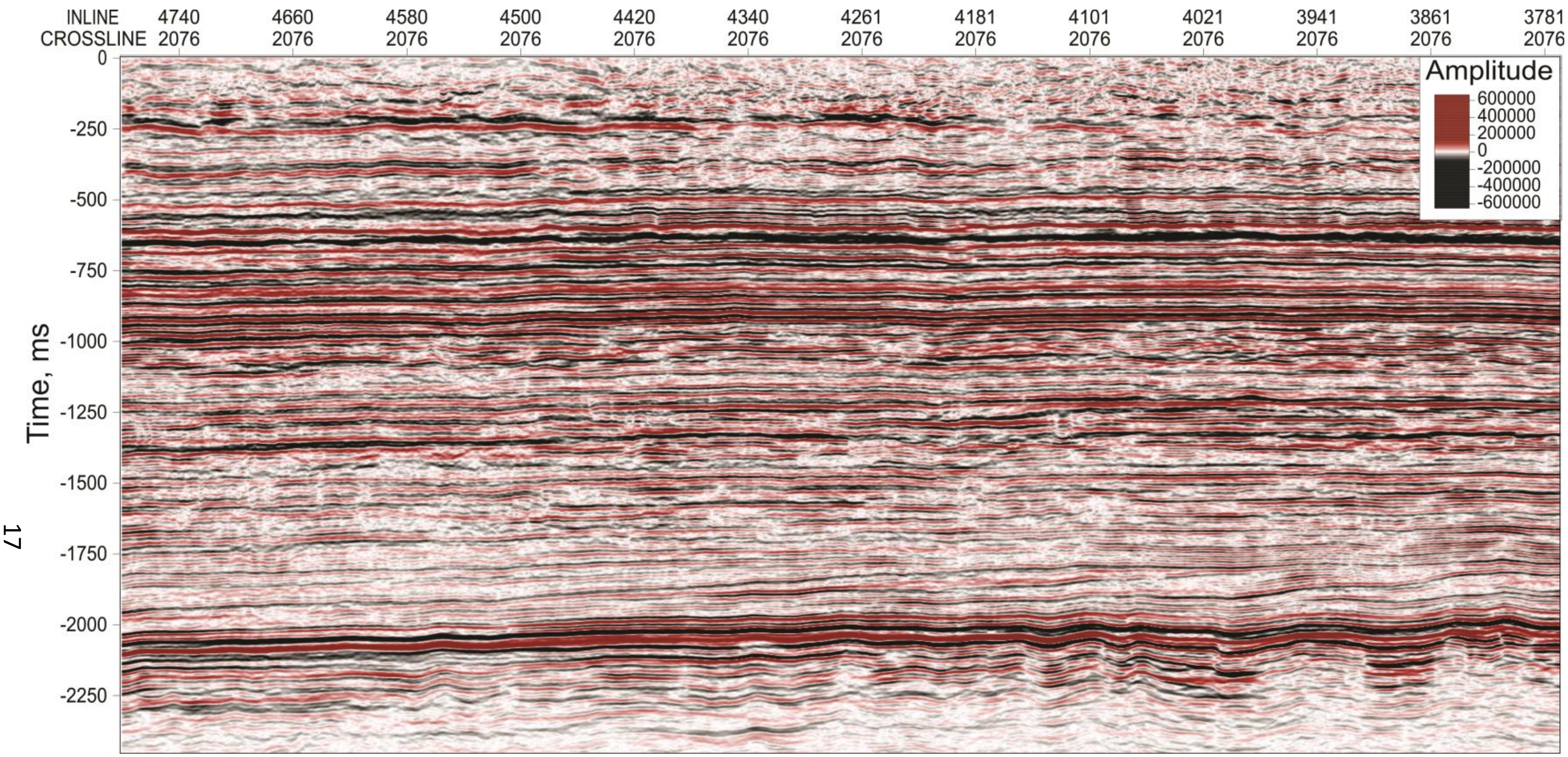

Figure 2.6 Crossline 2076: sufficient signal to noise ratio is observed.

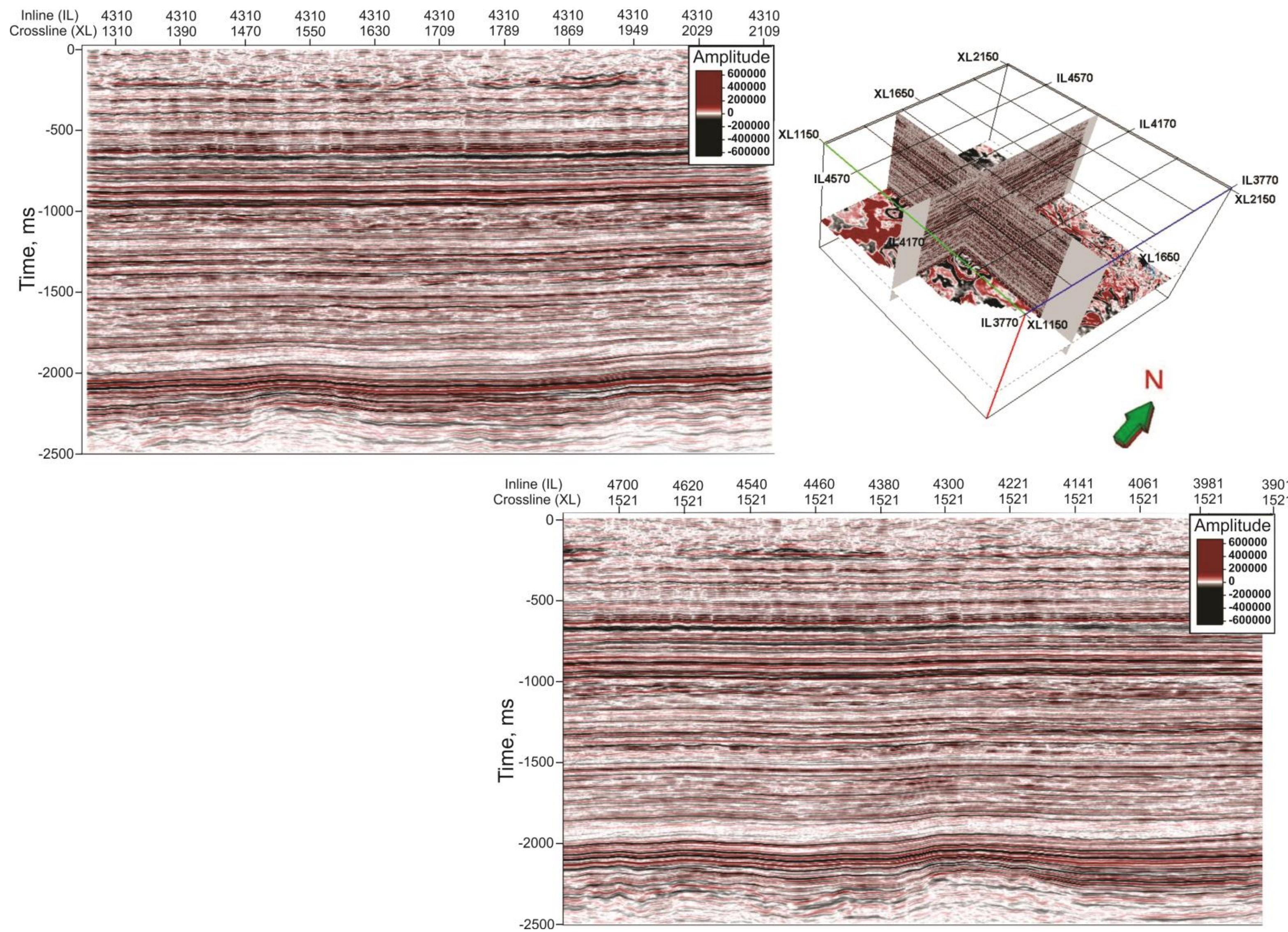

Figure 2.7 Schematic representation of inline 4310 and crossline 1521

Seismic data interpretation. Seismic data were tied to well-log data. For this purpose, the spread of the checkshot obtained from vertical seismic profiling (VSP) to the closest wells was made. In order to calculate synthetic seismograms, acoustic and density logs were used. In case of sonic logging absence, the resistivity log was recalculated in the sonic log. Generating the synthetic seismograms is a very important process, as it allows for the connection of the geological information (well data in depth) and geophysical information (seismic in time). The seismic well-tie-to-time section included the following steps:

1) Calculating the reflection coefficients through the acoustic and density logs;

2) Generating the synthetic seismogram by the convolution of the reflection coefficients with the wavelet-in this work the Ricker wavelet at 28 Hz was used;

3) Transforming the resulting synthetic trace in the time line and comparing with the seismic trace;

4) Aligning the synthetic seismogram to the seismic data to improve the tie between the seismic and well data and to improve the estimated wavelet.

The resulting correlation coefficient between the synthetic and seismic seismogram is 0.78 (Figure 2.8). Thus, based on the procedures above, a seismic well tie was properly made to connect the seismic and well log data.

The next step of the interpretation was to pick seismic horizons on the basis of geological markers that correspond to the key bed and target layers according to the seismic well tie. Horizon B (the top of the Upper Jurassic, Bazhenovskaya formation) is clearly allocated within the section. It extends over the study area and has the most expressed dynamic characteristics. Horizon B is characterized by stable amplitude of the negative phase and corresponds to the interval of 2000 - 2130 milliseconds of two-way time. Therefore the picking of horizon B is quite straightforward in contrast to the horizons of the Ju_3 and Ju_4 formations. The picking of reflection horizons for Ju_3 and Ju_4 presents certain difficulties due to the abrupt change of reflection intensity and instability of the frequency content. Therefore the correlation of target reflectors is difficult and qualitative. Figure 2.9 shows the seismic well tie where the Ju_3 horizon is associated more with zero than with through crossing, and the Ju_4 horizon is associated with peak.

Due to the thinness of the layers these horizons actually belong to one event, so it does not make sense to divide them into two separate formations. Thus, in this paper the interval Ju_3-Ju_4 is considered as a single formation.

The next stage of the interpretation was to build time structural maps. Figure 2.10 shows a time structural map of the surface of the Ju_3 reservoir with wells, which revealed the layers $Ju_{3\text{-}4}$ with different fluid saturations (oil, water, and water with oil).The structural factor can explain fluid saturation in the area of the wells 1, 5, 6, and 8. Thus, well 6 revealed a water-saturated part of the formation Ju_3 that is deeper than wells 1, 5, and 8, which revealed an oil part of the same formation.

However, the structure factor does not work in the area of wells 2, 10, 11, 12, or 13. In this case, it is necessary to consider not only the structural and structural-lithological factor, but also the difference in the physical properties of the reservoir at the different fluid saturations.

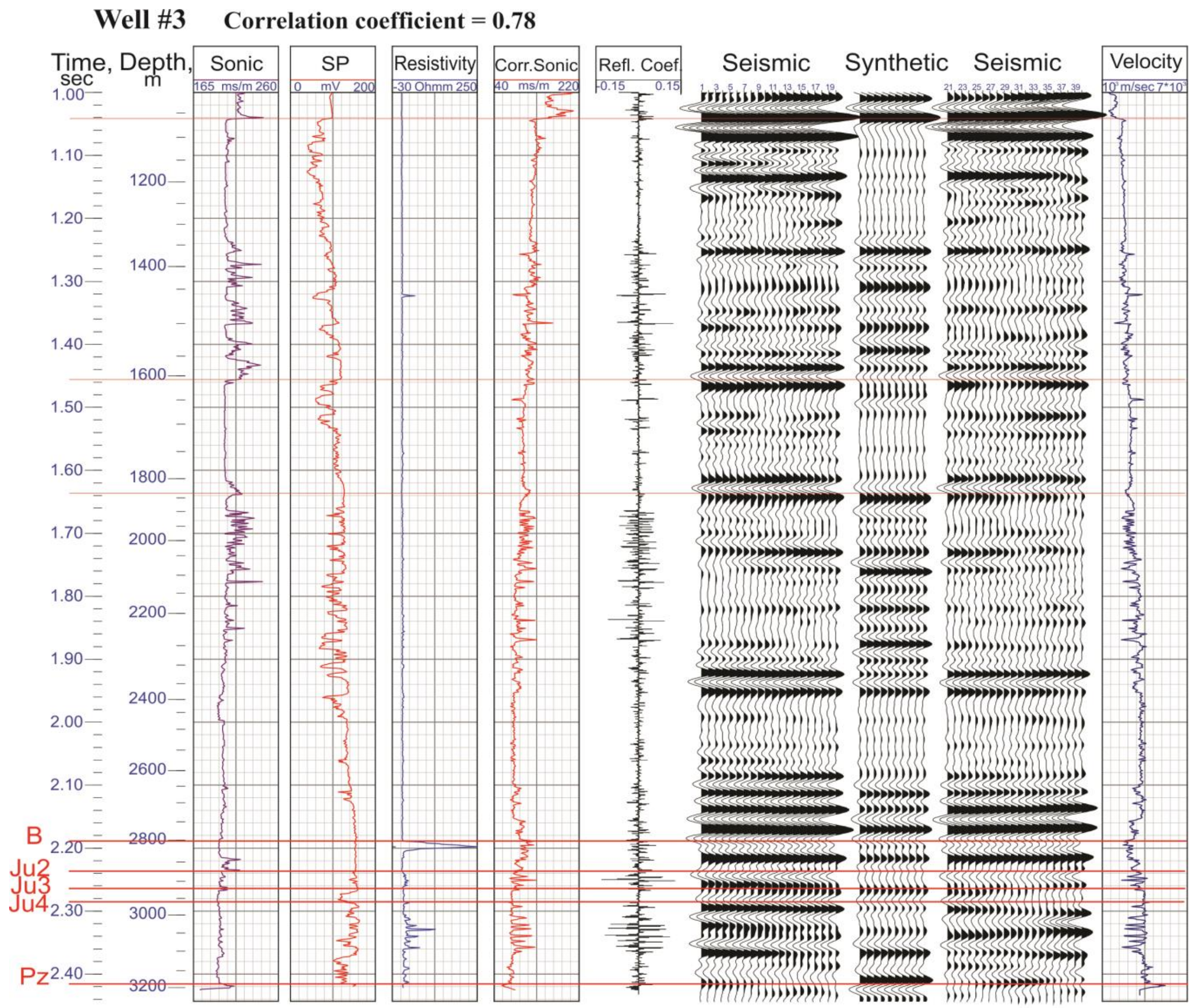

Figure 2.8 Seismic well tie of the well 3, correlation coefficient 0.78

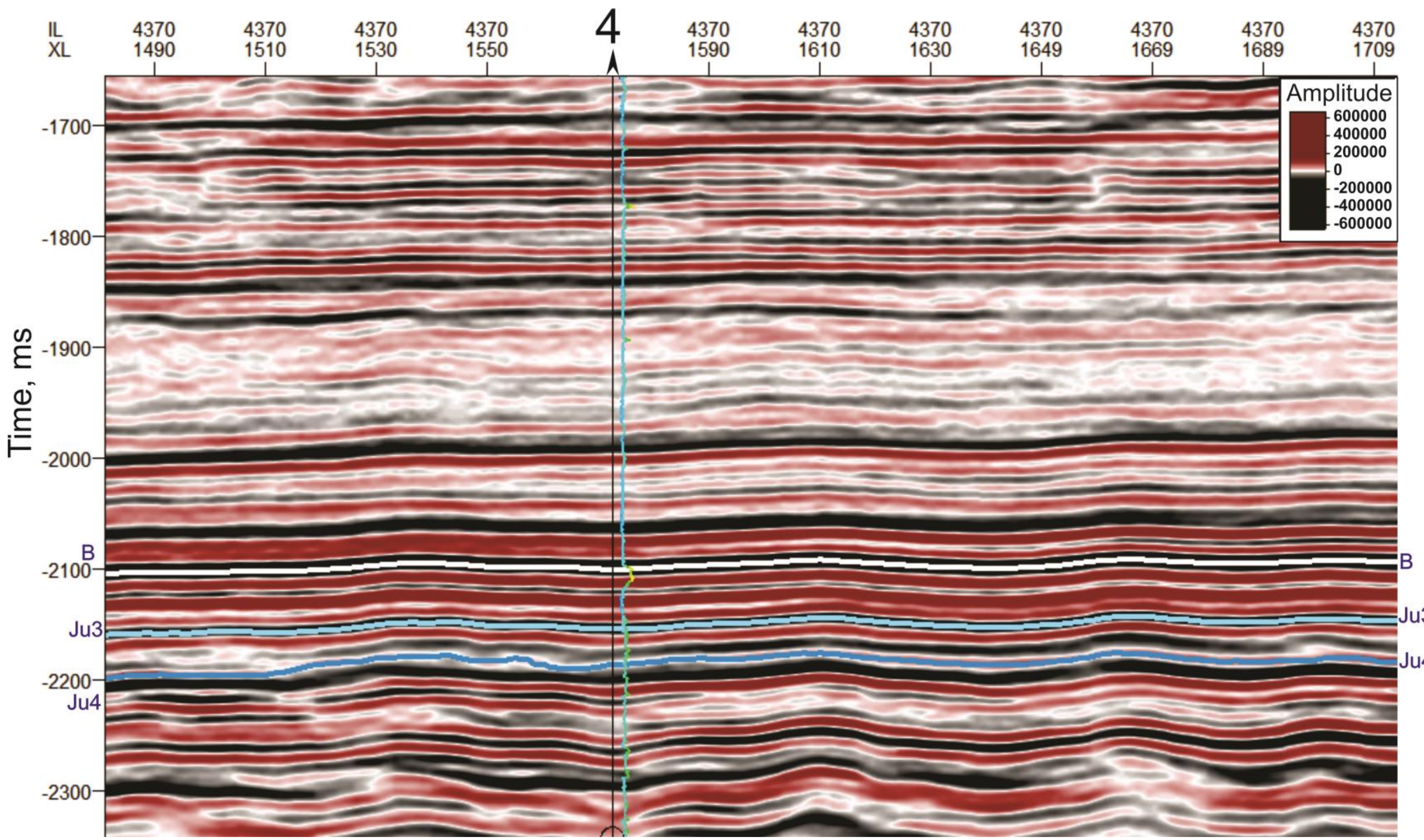

Figure 2.9 A vertical seismic section with picked horizons B, Ju3, and Ju4.

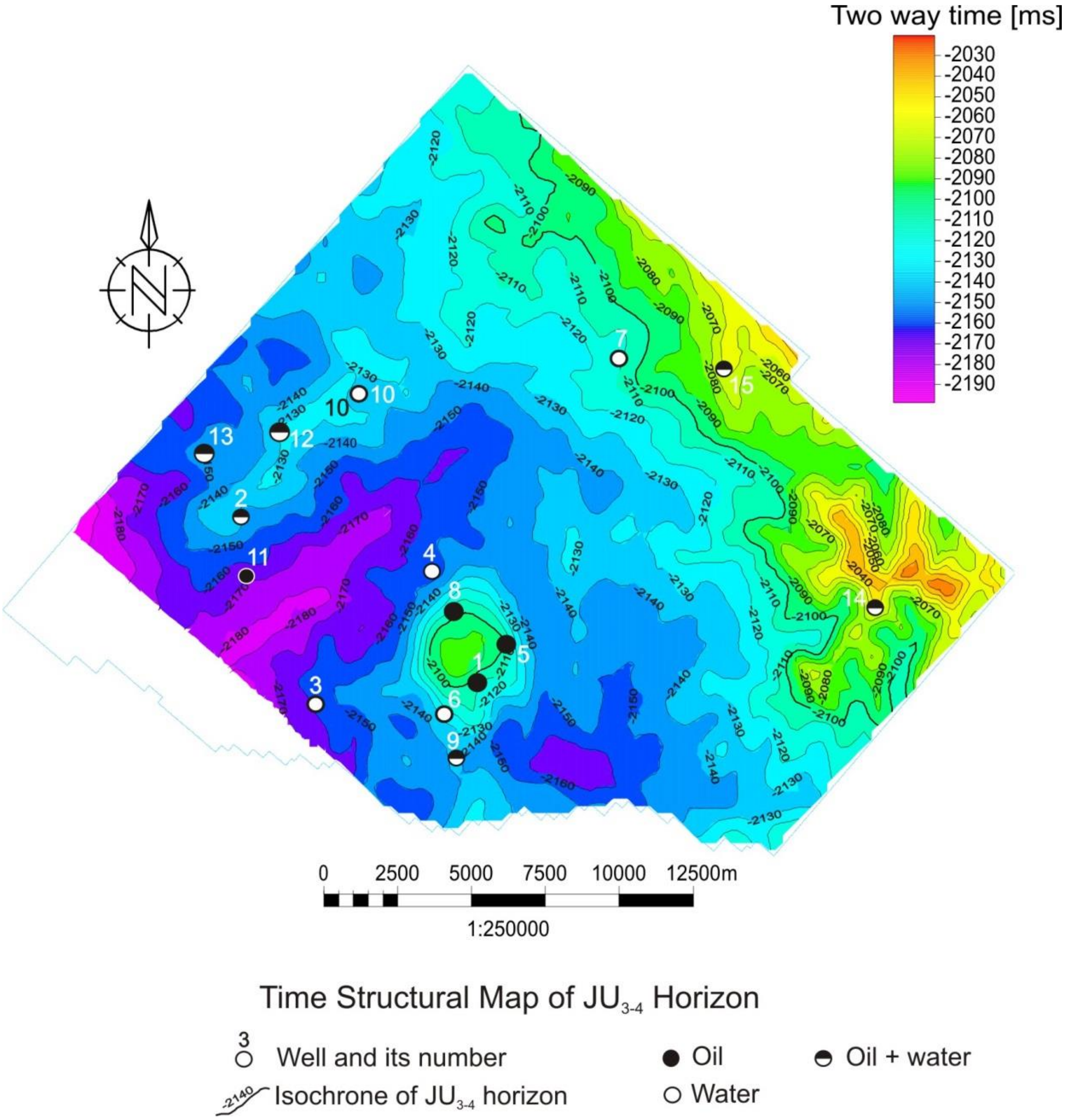

Figure 2.5 Time structural map of the surface of the Ju3-4 formations and location of the wells with different fluid saturation.

2.4 Petrophysics

The Middle Jurassic $Ju_{3\text{-}4}$ formation is characterized by very strong differentiation of lithological properties. The bed thickness varies from 45 meters to almost complete absence, and reservoir properties vary from highly porous, highly permeable reservoirs to almost sealed-off cemented impermeable rocks. According to the well-logging results, the porosity varies between 12-15% and can reach 20% or more in separate interlayers. Permeability may vary from 3-4 millidarcy (mD) to 40-50 mD, and there is a change in density from 2.03 to 2.17 g/cm^3. The results of the $Ju_{3\text{-}4}$ formation's well testing showed that there is a flow of oil in four wells, water in five wells, and oil with water in six wells.

Figure 2.11 shows a geologic cross section through the wells 6, 1, 8, and 4 with different fluid saturation correlating the major Jurassic formations. Bituminous clays of the Bazhenovskaya Formation (B), which lie above the $Ju_{3\text{-}4}$ formation, are shown clearly on the section. The Bazhenovskaya Formation clays differ from the underlying and overlying rocks by a high content of organic matter, chloroform bitumen, silicon, and high values of natural radioactivity, electrical resistivity, total porosity, and low density. The oil saturation part of the $Ju_{3\text{-}4}$ formation (wells 1, 8) is characterized by relatively low values of SP and increased resistivity of rocks in comparison with the water-saturated parts of these layers (wells 4, 6). Increased resistivity of reservoirs is one of the main criteria for identification of oil-saturated zones. This is a well-known sign of oil saturation that is uniquely observed in the $Ju_{3\text{-}4}$ formation. Figure 2.12a shows histograms of resistivity in the oil-saturated and water-saturated $Ju_{3\text{-}4}$ formations. The histogram illustrates that there is a fairly unambiguous separation between relatively low resistance of the water-saturated zones and high resistance of the oil-saturated intervals within the analyzed layers with resistivity's cut-off of 15-20 ohms.

Analysis of density and sonic log data shows that the difference between the densities of oil-saturated and water-saturated layers is noticeable (Figure 2.12b), whereas there is almost no difference between these layers based on interval time (Figure 2.12c). Obviously, the oil saturation decreases the density of porous rocks in relation with the water saturation. This decreases the bulk modulus of these rocks. However, interval time (P-wave velocity) in the Ju_{3-4} is practically independent of the fluid type due to the compensation of the bulk modulus changes because of the density variation.

By analyzing the density and acoustic properties of the Middle Jurassic formations, it can be stated that the following properties are typical for the Ju_{3-4} reservoirs: (1) the correlation of density with fluid type and (2) the lack of the dependence of the P-wave velocity on the type of fluid, and therefore, a weak differentiation acoustic impedance (slightly lower values of the acoustic impedance relative to the cap rocks).

Also, in order to evaluate the amplitude properties of the reservoir, distributions of acoustic impedance and C33 stiffness tensor parameter were built based on the log data. Figure 2.13a shows the distribution of the acoustic impedance in the oil-saturated and water-saturated zones of the Ju_{3-4} formation. The histogram shows that the difference between impedances of the oil-saturated and water-saturated reservoir zones is noticeable, but it is difficult to make an accurate separation between them. This was expected from the density and interval time analysis. Thus the use of values of acoustic impedance in order to separate oil-saturated zones from water-saturated zones is quite difficult. At the same time, the distribution of C33 stiffness tensor parameter (Figure 2.13b) shows a good separation between oil-saturated and water-saturated zones, which allows for the allocation of areas with different fluid saturation. These results will be used for the further analysis.

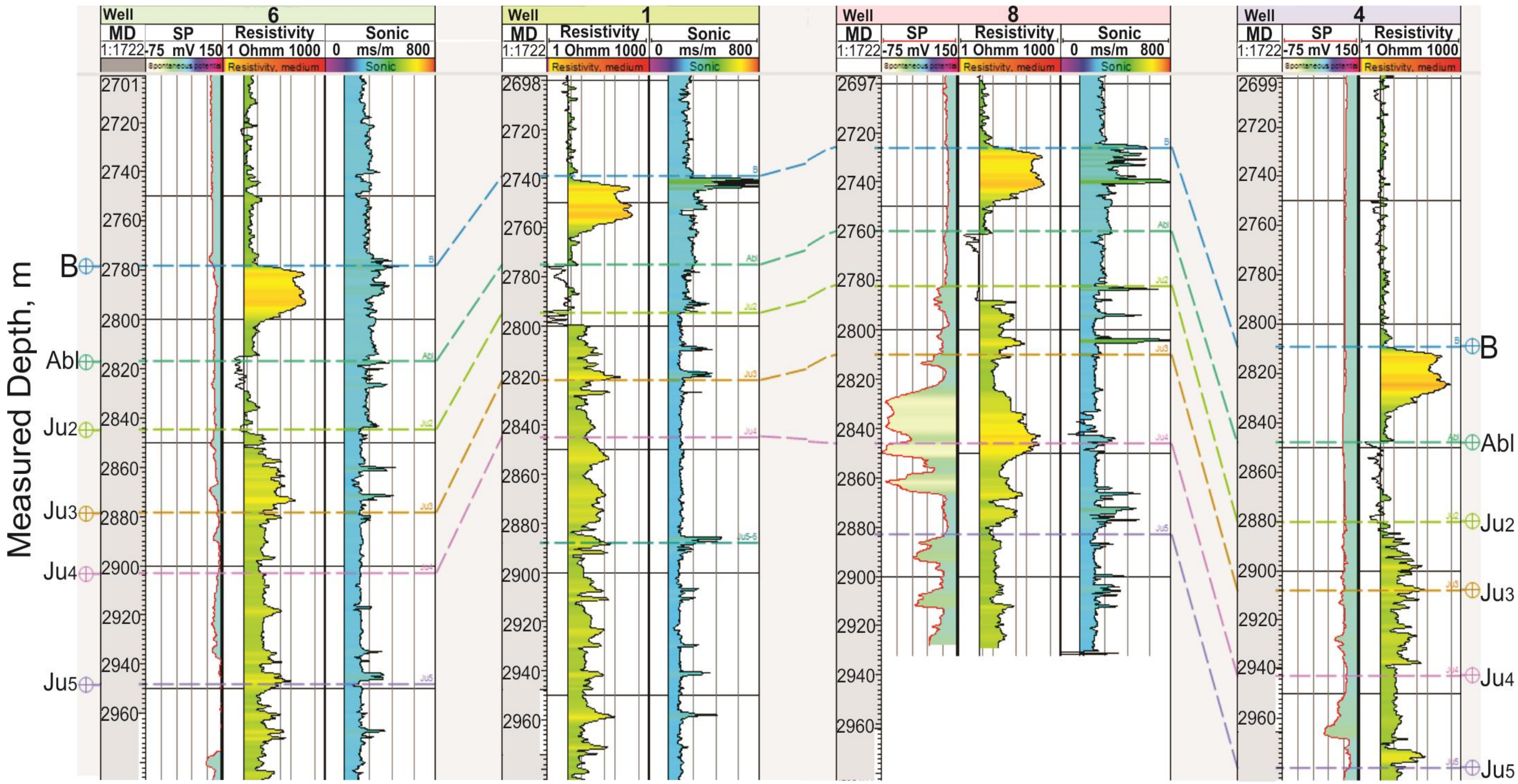

Figure 2.6 Geological cross-section over wells number 6, 1, 8, 4. The Bazhenovskaya formation (B) can be clearly distinguished by abnormally high resistivity values. Oil-saturated zones of the Ju3-4 formation have high resistivity values as well.

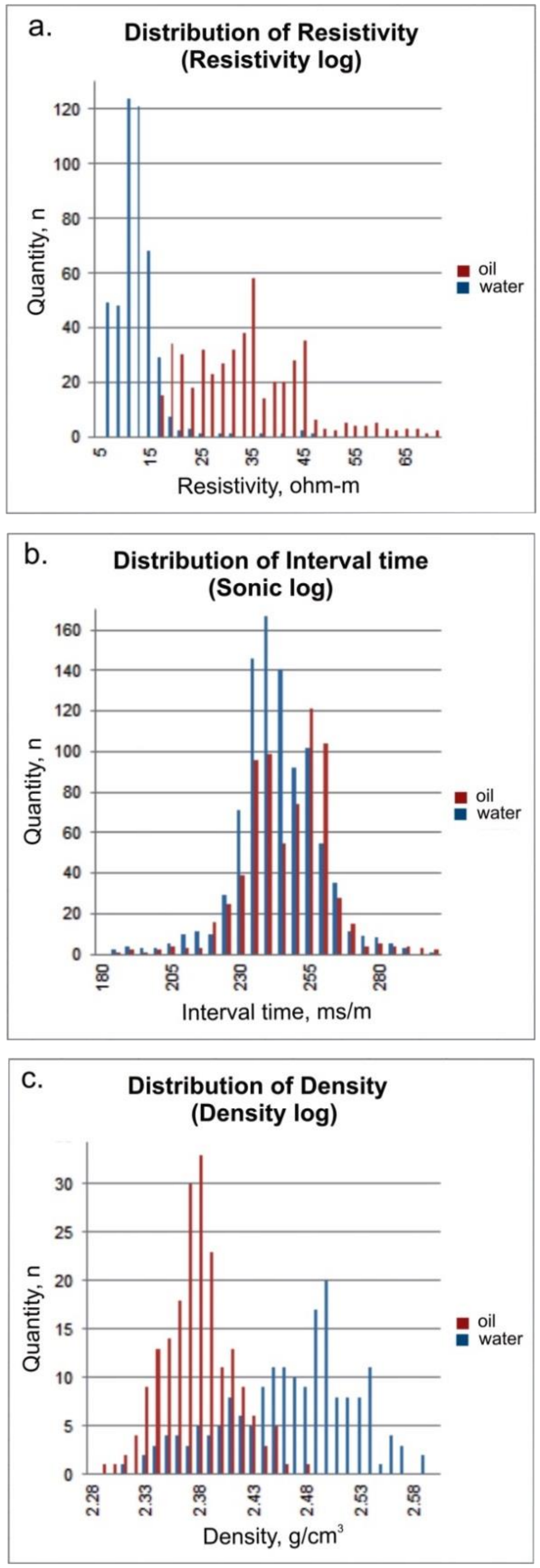

Figure 2.12 Histograms of (a) Resistivity, (b) Interval time, and (c) Density values, within oil- and water-saturated zones of the Ju3−4 formations based on log data.

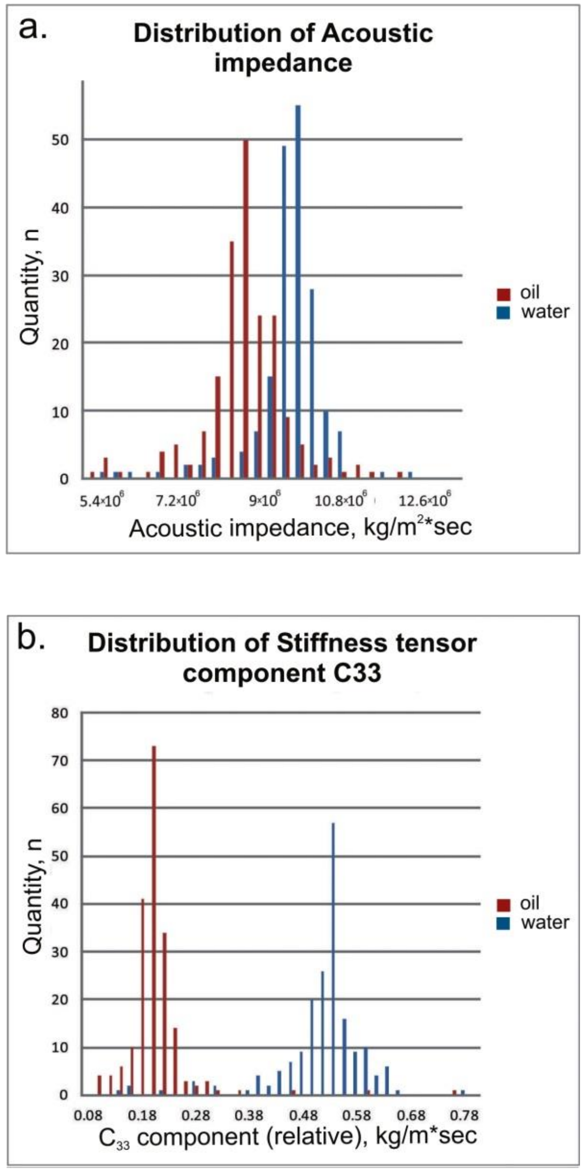

Figure 2.13 Histograms of (a) Acoustic impedance and (b) Stiffness tensor component C33 within oil and water saturated zones of the Ju3-4 formations.

CHAPTER THREE

AMPLITUDE ANALYSIS

3.1 Modelling

Amplitude analysis of seismic reflections has been used for a long time to not only understand the structural features of the studied area but also to find hydrocarbon deposits. There are many techniques for the amplitude analysis based on the different factors that could affect seismic amplitudes: layer thickness, lithological difference, fluid saturation, etc. This work is interested in using fluid-saturation-dependent amplitude changes to detect oil deposits. In the case of the Middle Jurassic formation we have to consider not only petrophysical and seismic properties of the Ju_{3-4} formation, but the properties of the Bazhenovskaya (B) formation as well. As previously mentioned, the bituminous clays of the B formation have a high impact on the dynamic characteristic of the wave from the Ju_{3-4} formation. Therefore, understanding the effect of the B formation on the reflections of the Ju_{3-4} formation is critical.

Figure 3.1 shows the acoustic impedance model for the B formation. The acoustic impedance of the B formation is considerably low compared to the overlying and underlying layers. This impedance contrast causes a strong negative reflection from the B formation. In case of the Ju_{3-4} reservoir model there is a gradual increase of acoustic impedances from overlying to underlying layers. Figure 3.2 illustrates the acoustic impedance models for the Ju_{3-4} reservoir in case of different fluid saturation. The oil-saturated part of the Ju_{3-4} formation has lower impedance than the water-saturated part due to a decrease in density and P-wave velocity of the formation. According to the Ju_{3-4} reservoir models, a seismic wave from the Ju_{3-4} is characterized by relatively weak reflections, which we previously observed on the seismic well tie (Figure 2.7).

Because the Ju_{3-4} formation is characterized by weak reflections, it is expected that the reflection wave from the B formation highly contributes to the wave from the Ju_{3-4}. Therefore, in order to predict fluid saturation using amplitude analysis of the Ju_{3-4} reflected wave, it is first necessary to decrease the influence of the strong reflections from the B formation wave. In other words, it is important to improve the signal-to-noise ratio, where the signal is represented by the reflections from the Ju_{3-4} and noise is the reflections from the B formation.

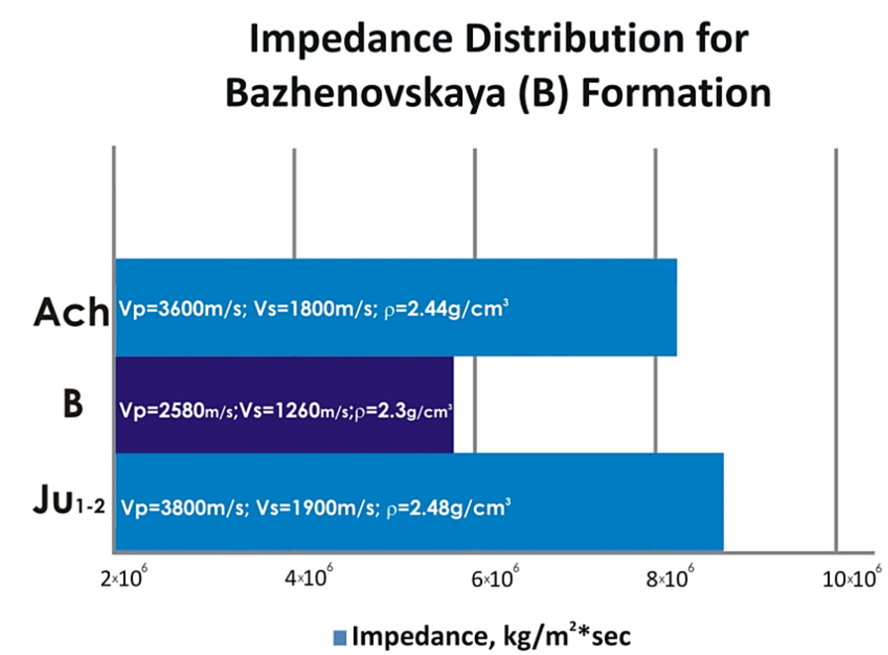

Figure 3.1 Impedance model for the Bazhenovskaya Formation.

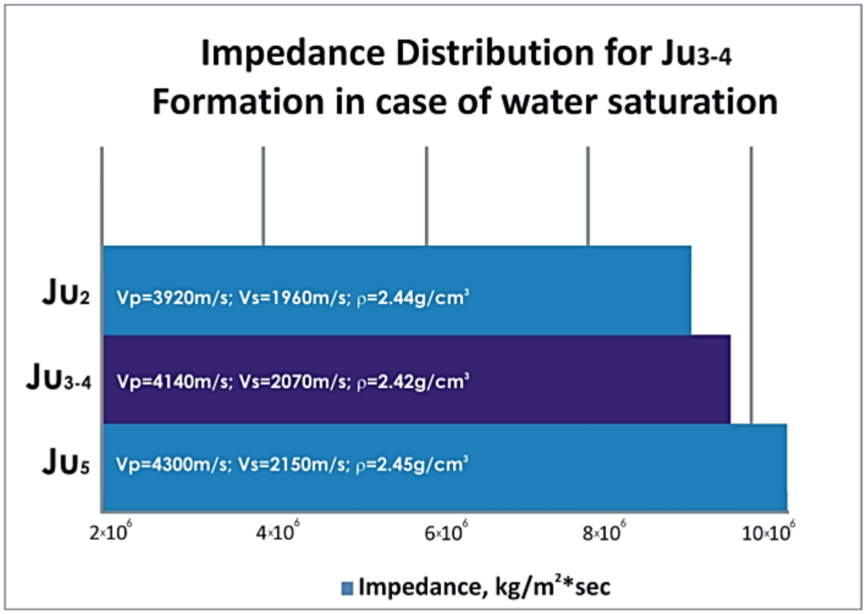

(a)

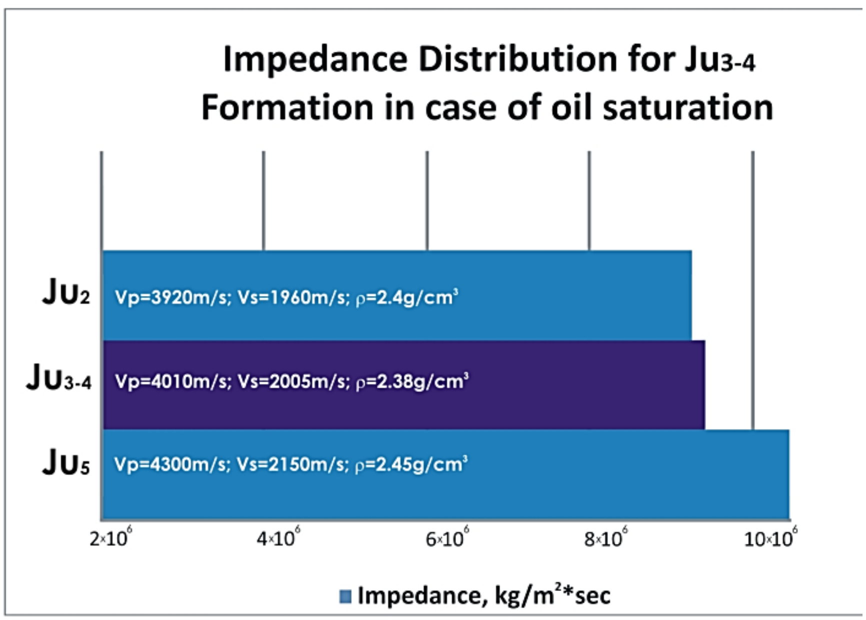

(b)

Figure 3.2 Impedance model for the Ju3-4 formation in case of water saturation (a) and oil saturation (b) of the reservoir.

For this purpose, frequency responses of the B and Ju_{3-4} reflections were calculated based on the impedance models of the B and Ju_{3-4} horizons in order to trace the behavior of seismic signature with changing frequency (Figure 3.1). The results are presented in Figure 3.2.

The calculations took into account the frequency response of a 10Hz geophone used for field work (Figure 3.2 b), which was obtained using the formula (Boganic et al., 2006):

$$G(\omega) = \frac{\mathrm{ap}^2}{\sqrt{(1-p^2)^2+4b^2p^2}}, \tag{3.1}$$

where $p = \frac{\omega}{\omega_0}$ and $b = \frac{a}{\omega_0}$ are relative values of the harmonic oscillation's frequency and damping ratio respectively as compared to the natural frequency; $a = \frac{\omega}{\sqrt{2}}$ is an optimal damping factor. The calculation results show that the signal/noise ratio can be expected to be high in the geophone resonance region, i.e., in the range of 10Hz. Hence, it makes sense to apply amplitude analysis and consider seismic response from the Ju_{3-4} reservoir in the low-frequency domain.

The combination of different interpretation methods is often applied in dealing with complex geological tasks. In this work, in order to detect the oil saturation, the amplitude variation with offset (AVO) and frequency-dependent (FD) analyses are applied. The following formula for the reflection coefficient for the layer is used (Brekhovskih, 1957):

$$R = \frac{R_1 + R_2 e^{i\omega \Delta t cos \theta_2}}{1 + R_1 R_2 e^{i\omega \Delta t cos \theta_2}} \quad , \tag{3.2}$$

where $R_1 = R_{12}$ is a reflection coefficient of the overlying layer, $R_2 = R_{23}$ is a reflection coefficient of the underlying layer, Δt is the time thickness of the layer equal to Δt = 2d/V, where d is a thickness of the layer and V is velocity, Θ is angle of incident (Figure 3.3). In case of a normal incident the formula takes the following form:

$$R = \frac{R_1 + R_2 e^{i\omega \Delta t}}{1 + R_1 R_2 e^{i\omega \Delta t}} \tag{3.3}$$

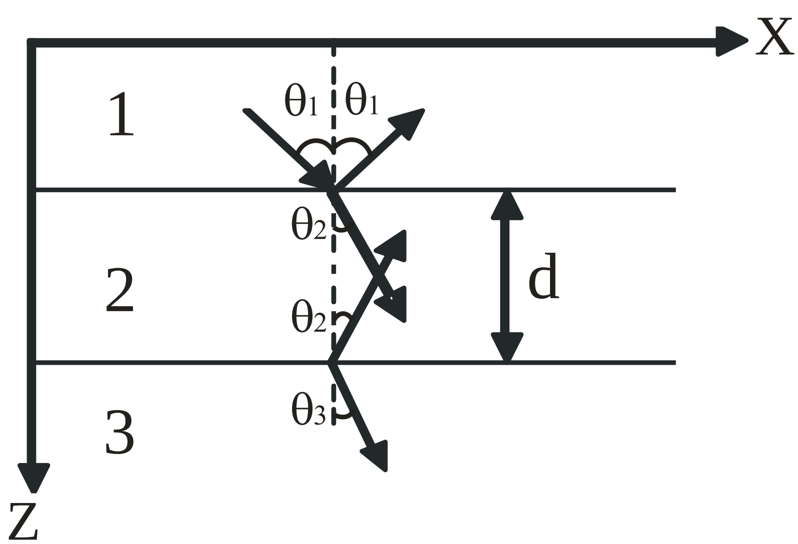

Figure 3.3 Schematic representation of the reflection of a plane wave from a layer.

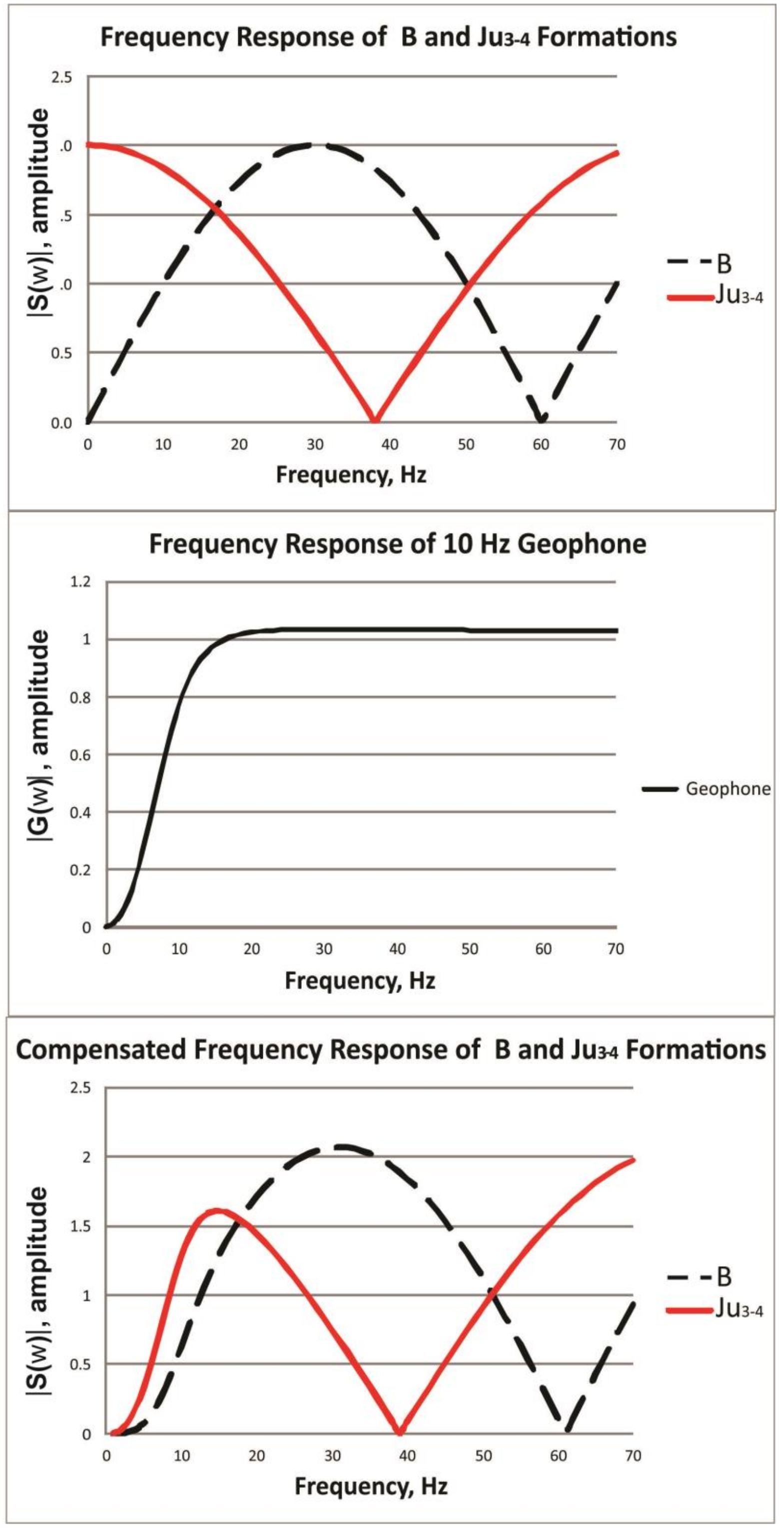

Figure 3.4 Frequency response of the B and the Ju3-4 formation before the compensation (a); frequency response of 10 Hz field geophone (b); frequency response of the B and the Ju3-4 formation after the compensation due to the 10 Hz geophone (c).

3.2 Amplitude versus offset

One of the most helpful techniques in the determination of fluid saturation is the amplitude variation with offset (AVO), which is based on measuring changes in seismic reflection amplitude as a function of the distance from source to receiver, or the angle of incidence. Therefore, the main idea of using AVO analysis is to explain the effect of fluid and rock variations on the seismic signature. The different fluid saturations alter the petrophysical properties of rocks, which lead to a change in acoustic impedance and reflection coefficient thereafter. AVO-anomaly classifications are based on the difference between acoustic impedance values of the reservoir and encasing medium. According to the model adopted in 1989 by Rutherford and Williams, and then supplemented by Castagna et al., 1997, there are 4 classes of AVO anomalies.

The first class is characterized by a high-impedance reservoir compared with the surrounding rocks. It is usually represented by mature, moderate, compacted on-shore sands. This type of sand has a high reflection coefficient value at normal incidence which then decreases in magnitude with offset or angle. The second class of AVO anomaly corresponds to compacted and consolidated sands that have almost the same impedance as the encasing rocks. Here the magnitude of the gradient usually increases when increasing the offset or angle, but can decrease as well. The second class of anomaly could not be detected on the stacked section and on the small offsets because the noise level can suppress the anomaly. Phase reversal is characterized by this class. The third class of AVO anomaly is known as bright spots. It has lower impedance than the surrounding medium, and is usually characterized by unconsolidated, under-compacted sands. These AVO anomalies are noticeable on a stacked section and clearly stand out on the far offset (Rutherford et al., 1989). The fourth class of AVO anomaly has lower acoustic impedance than an encasing unit, and reflections decrease with the offset (Castagna et al., 1997).

In the case of the Middle Jurassic, we should expect to see the second class of AVO anomalies, associated with oil saturation. This assumption makes sense due to several reasons: First, the impedance of Ju_{3-4} does not differ much from the encasing medium that we observed in the reservoir model of Ju_{3-4} (Figure 3.2); second, the fact that there is a noticeable separation between oil-saturated and water-saturated zones in the distribution of stiffness tensor parameter C33 (Figure 2.4c) could affect the AVO anomaly; and third, the Ju_{3-4} formation is represented by dense and consolidated sandstones, which corresponds to the second class of AVO anomaly.

According to the previous modeling (Figure 3.3c) the reflected wave from the Ju_{3-4} horizon could be detected in the low frequency domain. In order to follow amplitude behavior versus angle at low frequencies (10HZ), the amplitude response model from the Ju_{3-4} formation was built as a function of angle for different fluids and thicknesses. The following formula by Smith, 1987, for calculating the reflection coefficient due to different angles was used:

$$RC(\theta) = \left(\frac{NI_p}{cos^2\theta}\right) - 2NI_s sin^2\theta \qquad (3.4)$$

assume that *Vp=2Vs,*

where *NIp* is a reflection coefficient of a longitudinal (P) wave at normal incidence; *NIs* is a reflection coefficient of a shear (S) wave at normal incidence; Θ is the incidence angle; *Vp* is P wave velocity; *Vs* is S wave velocity.

The analysis of amplitude variation with angles and varying thickness of $Ju_{3\text{-}4}$ layer shows that regardless of the layer thickness, normal incidence has the biggest separation of amplitudes between oil and water (Figure 3.5).

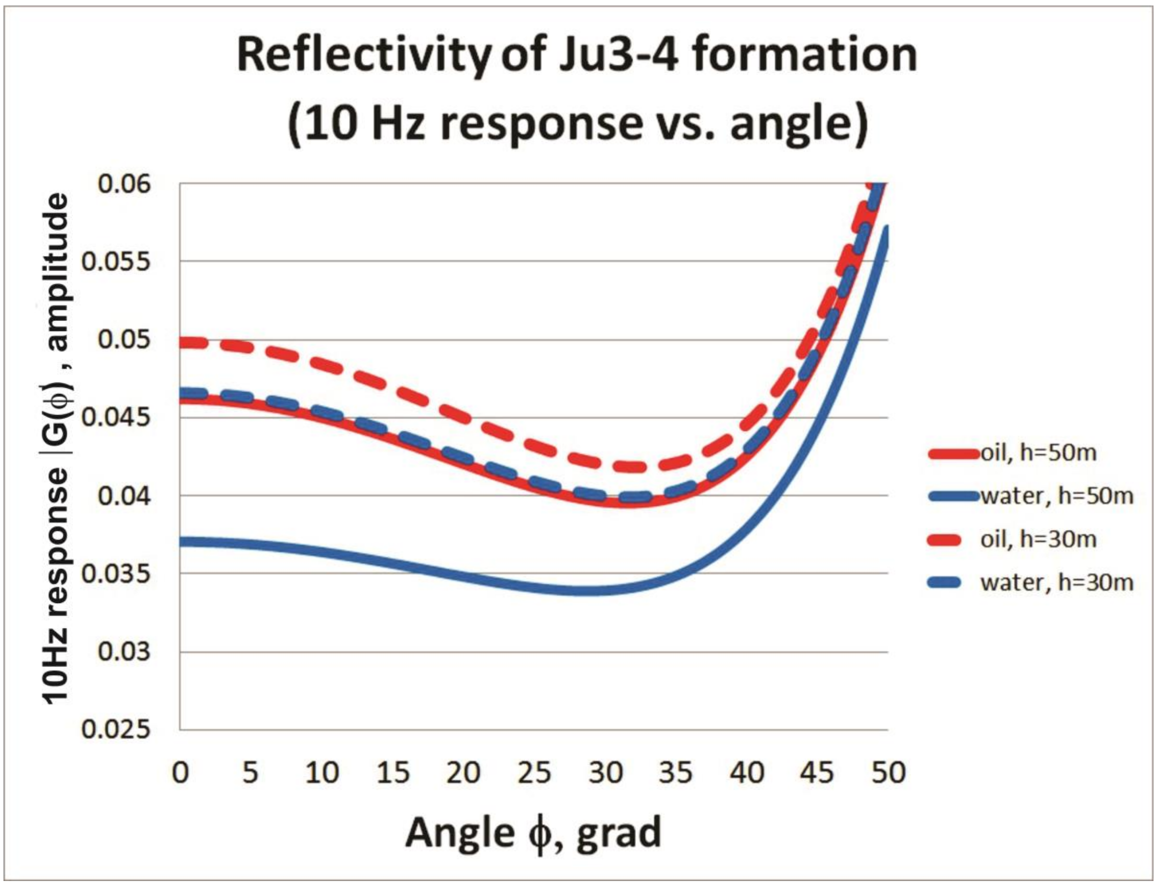

Figure 3.5 Frequency response (10 HZ) of the Ju3-4 Formation in case of different angle of incident at different thicknesses and saturation.

The testing of the amplitude behavior versus offset on the real data showed results that are consistent with the modelling. Figure 3.6 shows two gathers; one of them is registered near the wellbore with the water, and another is near the wellbore with the oil. The fact that the amplitude of the reflected wave from the oil-saturated zone in the Ju_{3-4} formations is slightly higher than the amplitude of the reflected wave from the water-saturated zone in the same formations is noticeable. However, we cannot affirm that this effect as a hydrocarbon signature as it is very slightly expressed. Also, a change of the amplitude versus offset (gradient) is not very different in either case. It should be noted how the high-amplitude reflected wave from the bituminous shales of the B Formation (horizon B) affects a relatively weak target-reflected wave from the Ju_{3-4} formation. The interference of the tail part of Horizon B's wave with the target wave distorts the dynamic characteristics of the latter. This distortion affects the AVO attributes (Figure 3.7), which are noisy and weakly-expressed in the reservoir interval. The seismic section (Figure 3.7a), sections of the intercept (Figure 3.7b), and the gradient (Figure 3.7c) all show low-efficiency use of the data when trying to indicate oil in the Ju_{3-4} reservoir within the study area.

These results from the AVO analysis are expected due to the geological characteristics of the Ju_{3-4} formation. In the case of highly compacted mature consolidated Jurassic sands there is no large effect of fluid compressibility on the whole rock compressibility, and as a result there is no considerable AVO anomaly (Simm et al., 2014). The presence of an intensive reflected wave from the B formation complicates the effect of the Ju_{3-4} formation and thus decreases the signal to noise ratio, which is important for the correct determination of AVO anomalies.

Therefore, when considering the low frequencies, it makes sense to apply frequency-dependent amplitude analysis since the amplitude versus angle technique will not give us additional information about fluid saturation.

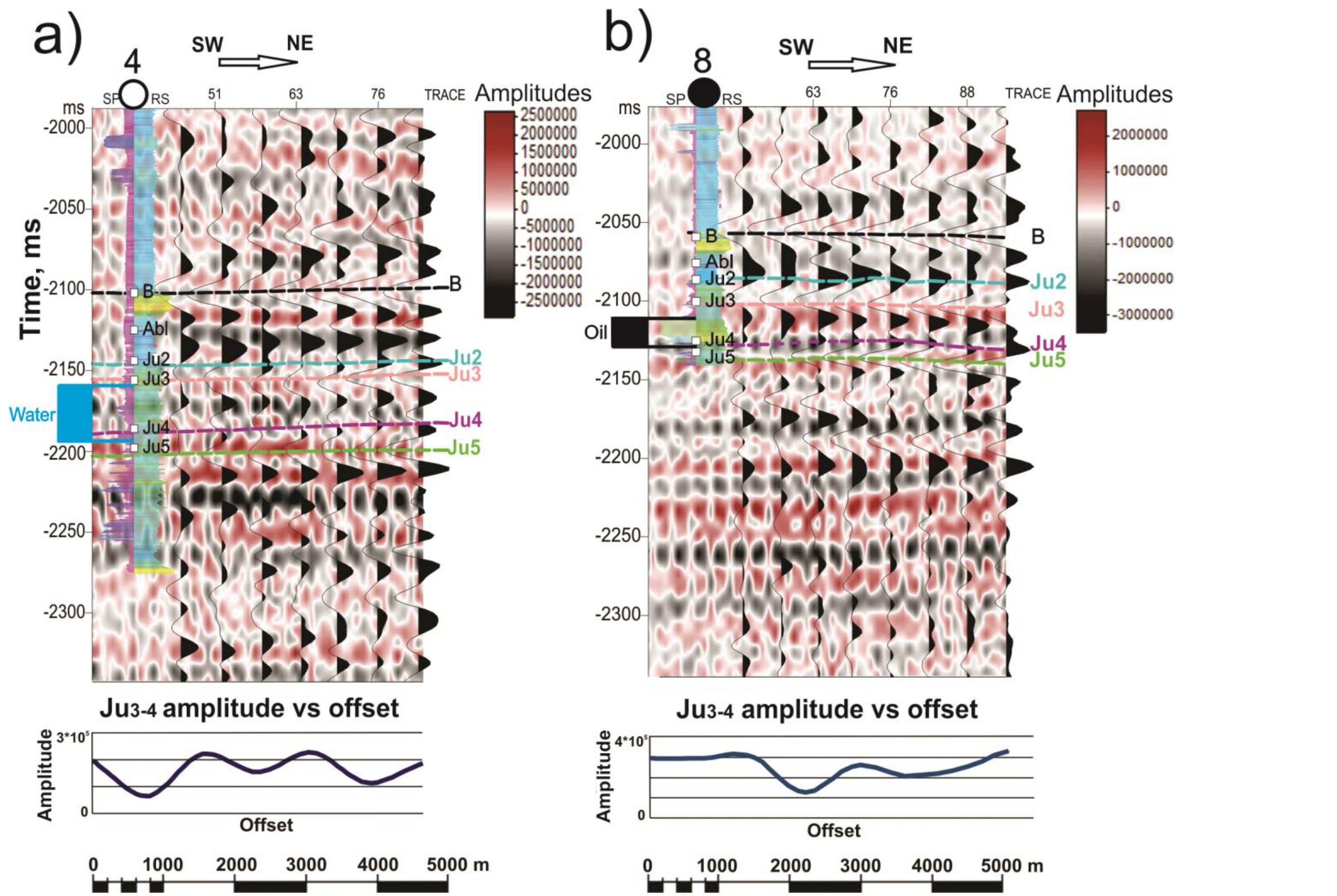

Figure 3.6 Pre-stack CMP gathers observed nearby (a) well #4 and (b) well #8. An amplitude level of the reflected wave from oil-saturated Ju3-4 interval is slightly higher than amplitude level in case of water saturation. There is no difference in gradients.

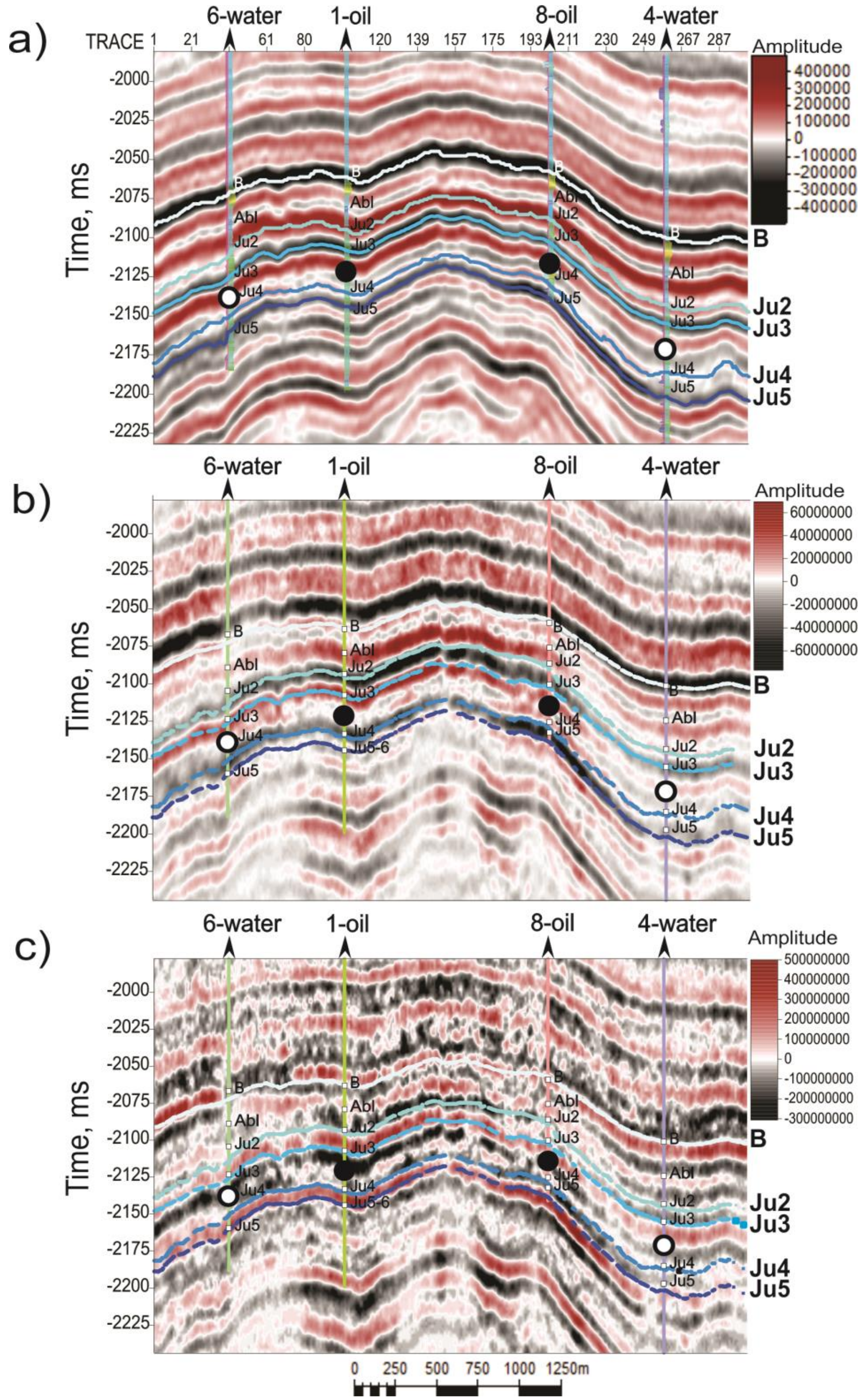

Figure 3.7 (a) Vertical full-stack seismic section, (b) vertical section of intercept, and (c) vertical section of gradient. Different types of fluid saturation for the Ju3-4 formation are showed by circles in the wells (black-oil, white–water).

3.3 Amplitude versus frequency

The effect of frequency on seismic amplitudes has been studied for a long time. Consideration of the seismic signal not only in time domain, but also in frequency domain provides new opportunities for data analysis. It is obvious that high frequencies give a higher resolution of the seismic image which is very efficient in the determination of geological structure; however, low frequencies could be an indicator of hydrocarbons. Taner et al., 1979, mentioned that a low-frequency shadow is observed below gas, condensate, or oil reservoirs. In 2003, Castagna et al. showed that gas deposits could be detected by the low-frequency shadow. A large number of works dedicated to this effect was carried out (Goloshubin et al., 1996; 1998; 2000; Korneev et al., 2004).

In the case of the Middle Jurassic Ju_{3-4} formation, the previous modelling (Figure 3.4) showed that the reflected wave from the Ju_{3-4} can be detected at low frequencies, as there will be minimum effect from the B formation, and consequently there will be a higher signal to noise ratio. However, it is important to consider the behavior of the Ju_{3-4} reflectivity, particularly in case of the different fluid saturations and varying frequencies. The result of Ju_{3-4} reflectivity versus angle (Figure 3.7) showed that the biggest difference existed between oil-saturated and water-saturated zones in the case of normal incidence. Hence, it makes sense to consider the Ju_{3-4} response from oil-saturated and water-saturated zones at normal incidence and varying frequency. Figure 3.8 illustrates the frequency characteristics of the reservoir Ju_{3-4} formation model with different saturations. At low frequencies the amplitude of the reflected waves from the oil-saturated layer exceeds the amplitude of the waves from the water-saturated layer. Therefore, applying frequency-dependent interpretation to the real data is reasonable.

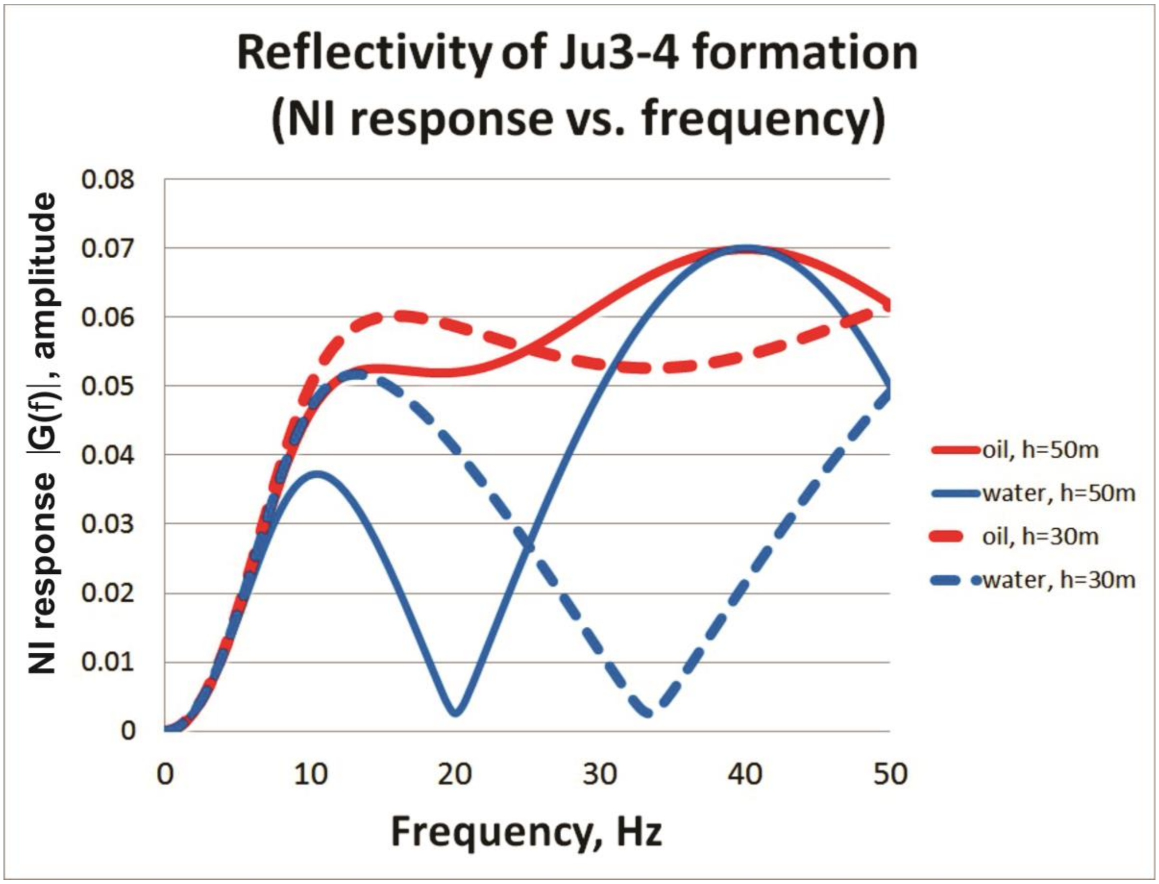

Figure 3.8 Frequency response of the Ju3-4 Formation in case of normal incidence and different frequencies at different thicknesses and saturation.

3.4 Spectral Decomposition

One of the most common methods of frequency-dependent amplitude analysis that proved itself useful as a tool for hydrocarbon detection is spectral decomposition (Castagna et al., 2003; Goloshubin et al., 2002; 2006). This method basically decomposes the seismic reflection data into separate frequency components found within the measured seismic bandwidth. Spectral decomposition of the wave field is a common method of the study for fluid-saturated reservoirs. This approach has been applied in seismic exploration for a long time.

Spectral decomposition allows researchers to distinguish different frequency components, which in turn help to study the effect of fluid saturation reservoirs. Therefore, the method of spectral decomposition converts seismic data from the time domain to the frequency domain. This procedure has a long history going back as far as Fourier, who in 1807 developed a method which showed that a signal can be represented by a series of coefficients obtained from an analysis function. The mathematical solution developed by Fourier underlies all currently existing spectral decomposition methods. There are many well-studied tools for spectral decomposition used in seismic data such as the Fourier Transform, Wavelet transform, and their modifications. For example, the Short Time Fourier Transform (STFT) converts the signal into a time-frequency spectrum by shifting a fixed-size window through the signal and taking the Fourier transform of the windowed portions (Cohen, 1995). The resolution of seismic data using this method has constraints due to the user-specified window length: too short of a window can bring unrealistic high frequencies, while too long of a window will have a narrow bandwidth in the frequency domain for the signal in time. In comparison, the Continuous Wavelet Transform (CWT) (Chakraborty and Okaya, 1995) uses a wavelet as the analyzing function. It decomposes the signal in the time domain into a time-scale domain using orthogonal wavelets that vary in length and frequency by a factor of two. The size of the scale plays an important role as decreasing the scale will increase the time resolution, which will result in a decrease of frequency resolution. The combination of STFT and CWT is the S-Transform, which is based on a moving and scalable localizing Gaussian function (Stockwell et al., 1996). It provides good time and frequency resolution. Each of these transforms has its own advantages and disadvantages, and as was pointed out by Castagna et al., 2003, there is no perfect method that would be universal for each model of the medium. The main task is to choose a method of spectral decomposition that will meet the necessary criteria for further interpretation.

For the case of the Middle Jurassic Ju_{3-4} sedimentary rocks, it is important for the selected spectral decomposition to provide a good frequency resolution in the low frequency domain. A good frequency resolution is necessary in order to: 1) tune out the interference from the intensive reflected wave from the horizon B effectively, and 2) preserve the amplitude differences associated with different fluid saturations in the reservoir. Both S-Transform (ST) and Continuous Wavelet Transform (CWT) meet these requirements.

Figure 3.9 shows the vertical full-stack seismic section through four wells with different fluid saturation (6 and 4 – water; 1 and 8 – oil) and with picked B, Ju_3, and Ju_4 horizons. The ST and CWT spectral decomposition methods were used on this seismic section. First, the S transform was applied to the section. Figure 3.10 illustrates the results from the S transform attribute at low frequencies and Figure 3.11 shows S transform at high frequencies of the full stack section. The reflected wave from the horizon B is most clearly imaged at high frequencies. Due to the tuning effect, the amplitude of the wave reaches a maximum at 30 Hz and weakens at both lower and higher frequencies. At 10 Hz the reflector from the horizon B is tuning out and, as a result, is poorly imaged. Exactly at 10 Hz, we observe a relatively strong reflector at the reservoir Ju_{3-4}.The amplitude anomaly of this wave corresponds to the oil saturation zone of the reservoir. The reason for such amplitude behavior is connected with a suppression of the interference effects from the Bazhenovskaya Formation. Therefore, we see the reflection from the Ju_{3-4} more clearly. These results are consistent with our obtained model (Figure 3.4).

Then, CWT was applied to the seismic data. Figure 3.12 and figure 3.13 show the results obtained at the same frequencies we used for the S transform. It is noticeable that major signatures exist, such as strong reflections from the B wave and anomalous amplitudes near the wells with oil at the Ju_{3-4} wave. However, the resolution of the low frequency images is much poorer in comparison with the results from the S transform. Since the objective is to have good resolution at low frequencies, i.e., where the reflections from the B wave have minimal influence, the results of the S transform are chosen for further analysis. Figure 3.12 shows the S transform result using a 10 Hz wavelet. The wave from the Ju_{3-4} formation is anomalous in amplitudes near the oil wells. It is possible to use the low-frequency (LF) attribute that can be created with the 10 Hz stack. This attribute should operate within the study area because the tuning out of the intense reflection of the B Formation at 10 Hz as the thickness of B formation is fairly consistent. Anomalous high values of the attribute will correspond to the oil-saturated zones and low values mean water-saturated parts of the area. Hence, it makes sense to calculate the LF attribute to the 3D seismic volume.

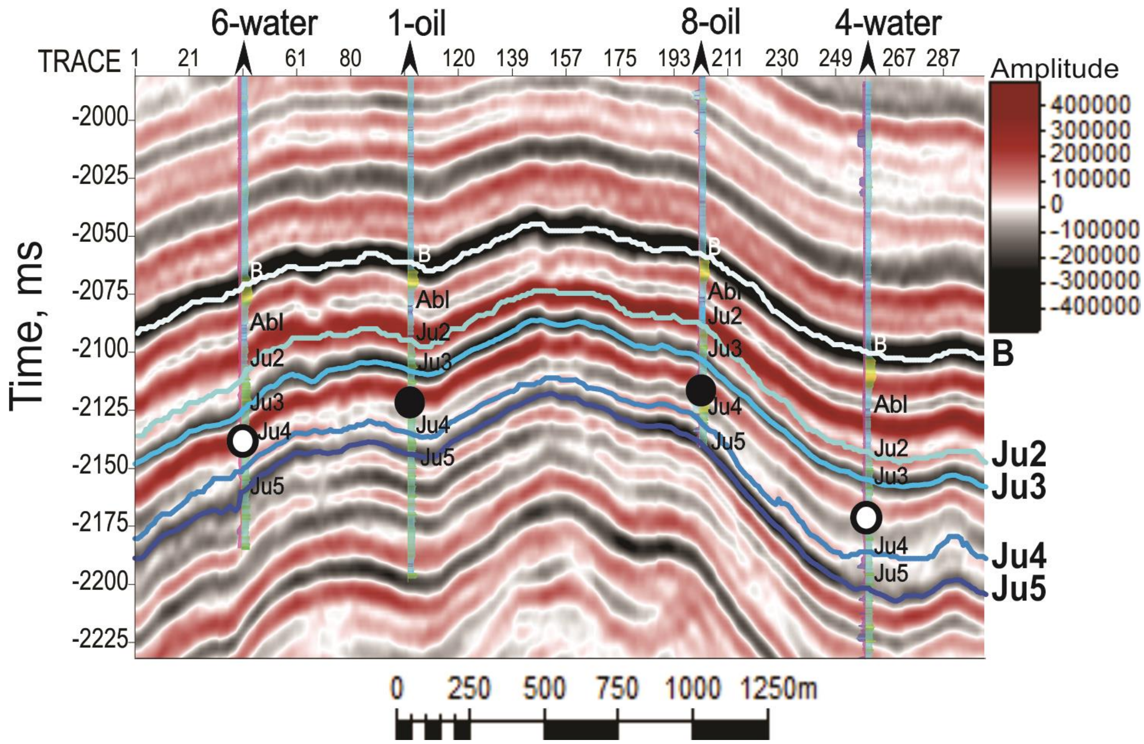

Figure 3.9 Vertical full-stack seismic section through wells with different fluid saturation (6, 4 – water; 1, 8 – oil) with picked horizons.

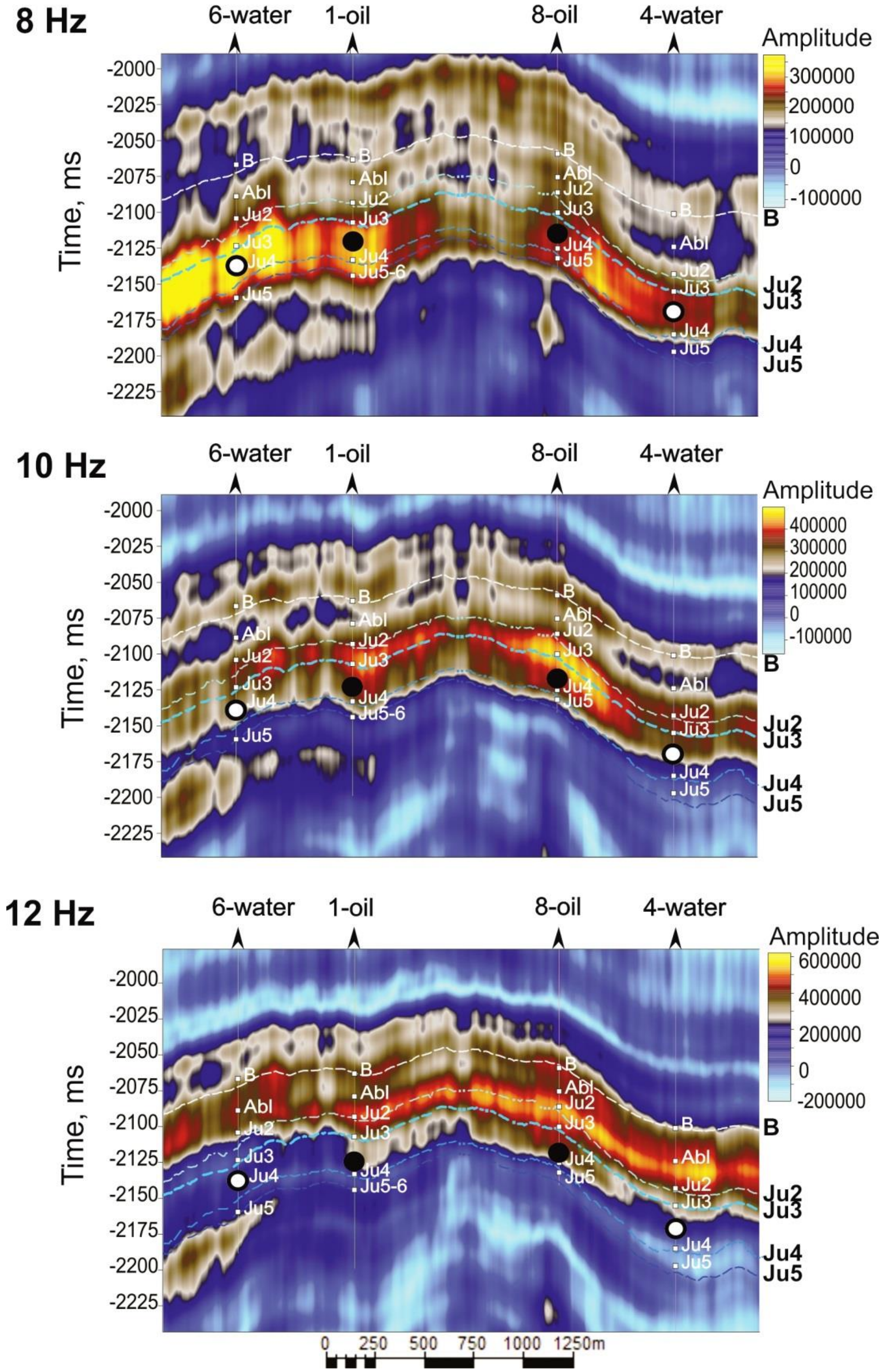

Figure 3.10 S transform's different wavelet forms of the seismic section at at low frequencies (8-12 Hz). The anomaly at 10 Hz fits oil saturated interval of the Ju_{3-4} formation.

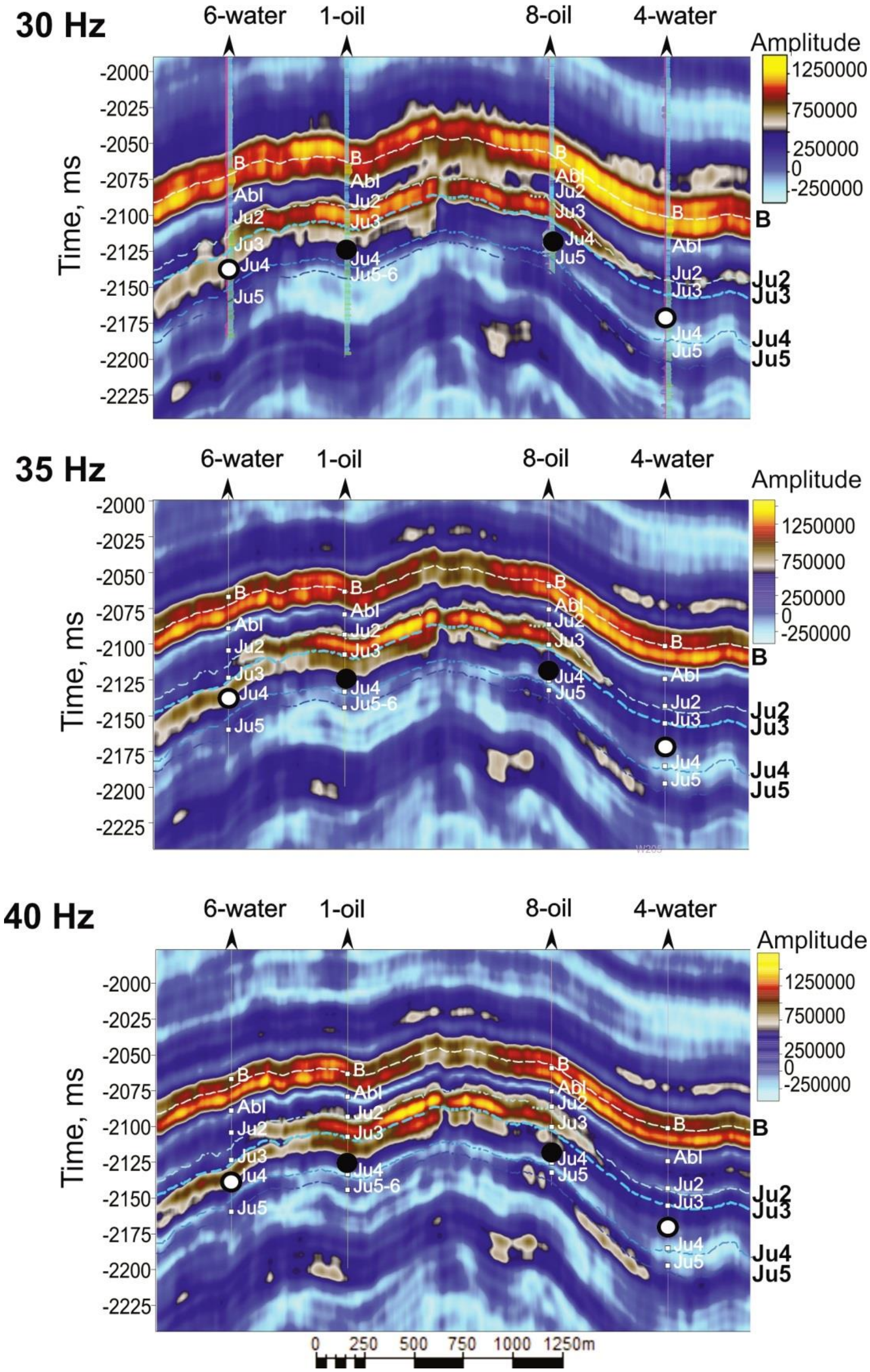

Figure 3.11 S transform's different wavelet forms of the seismic section at high frequencies (30-40 Hz). Sufficient resolution is observed.

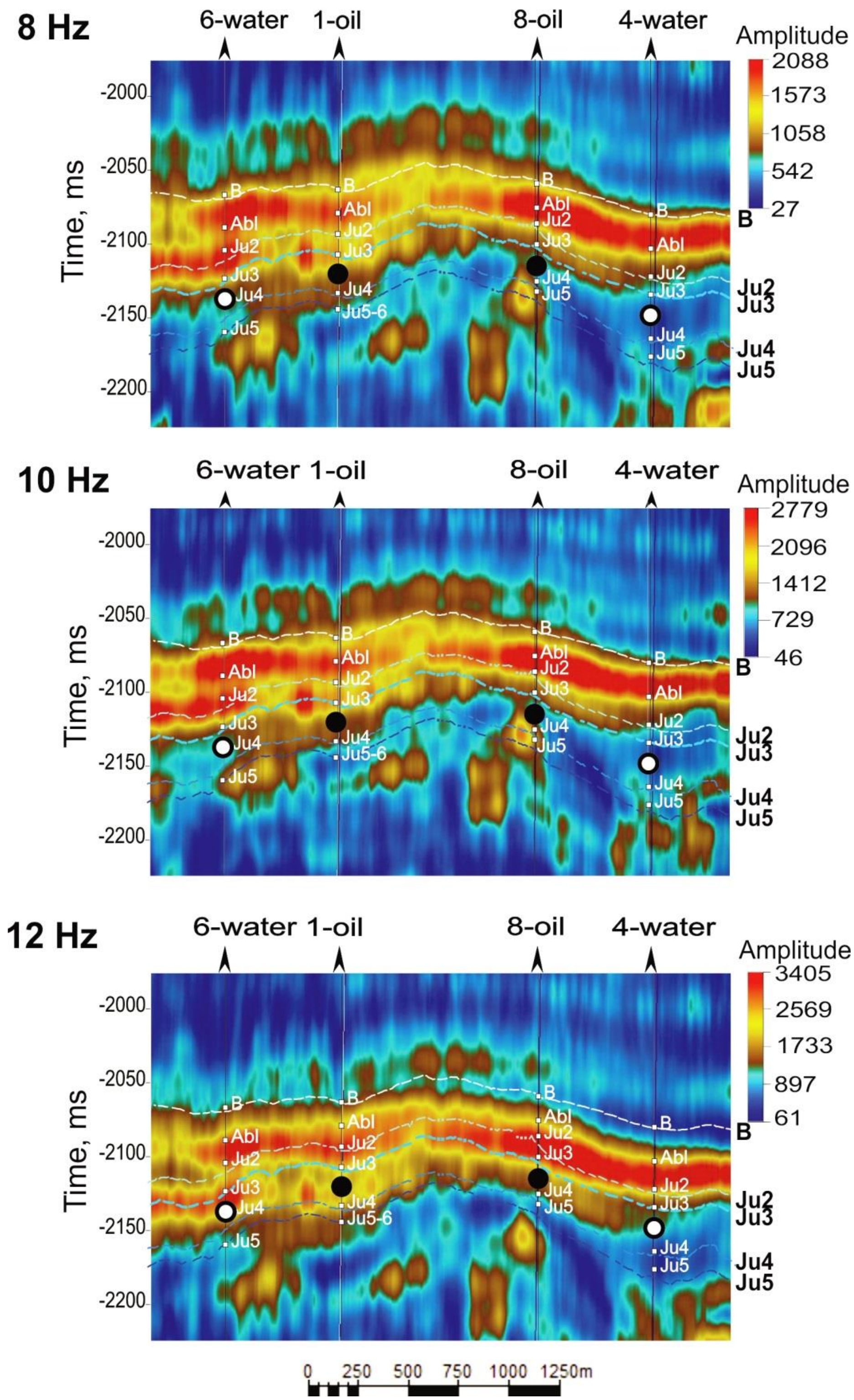

Figure 3.12 CWT transform's different wavelet forms of the seismic section at low frequencies (8-12 Hz). The CWT results have much poorer resolution at low frequencies which is sufficient for the suppression of "B" wave than S transform's results.

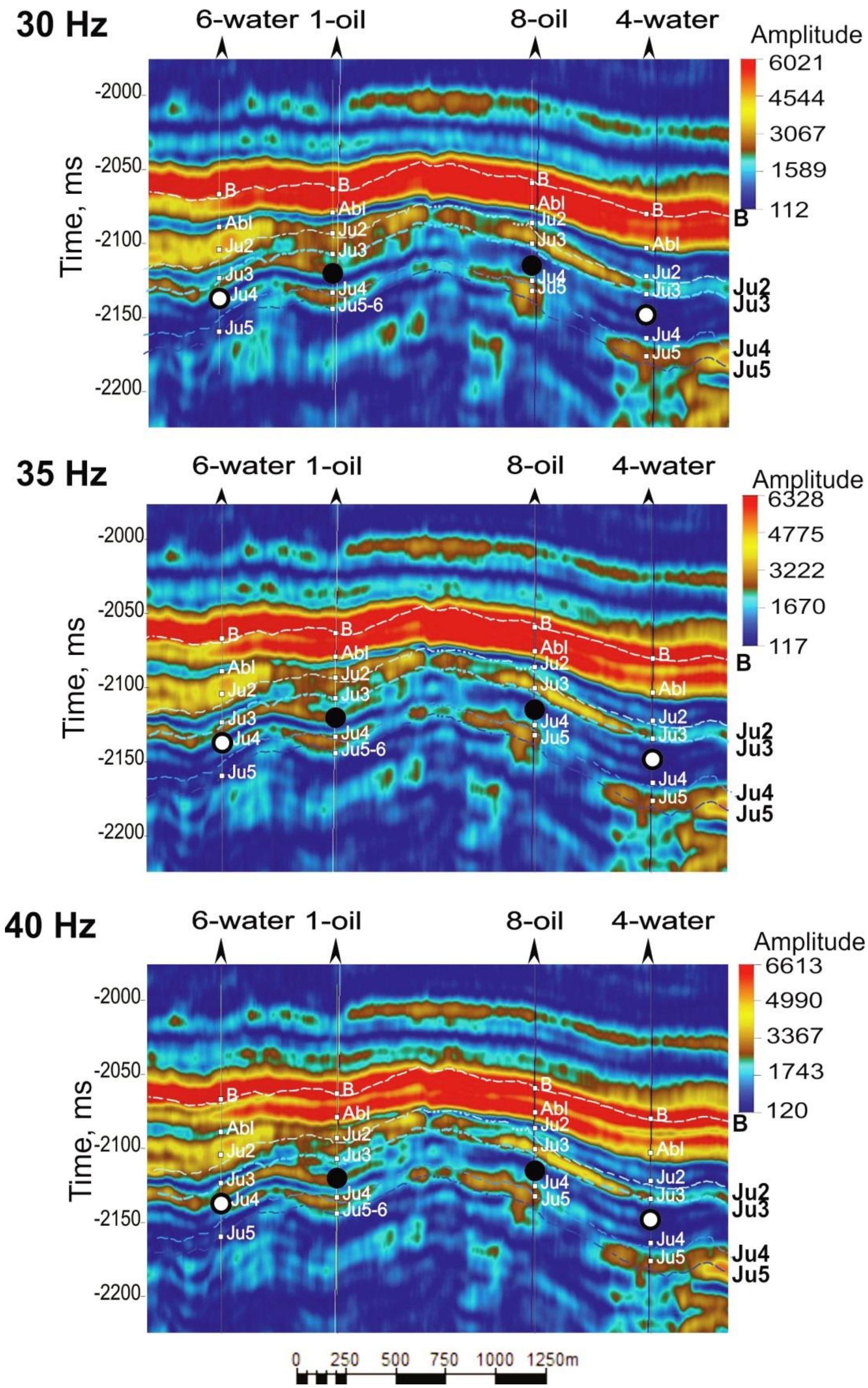

Figure 3.13 CWT transform's different wavelet forms of the seismic section at high frequencies (30-40 Hz). The CWT results have poorer resolution at high frequencies than S transform results.

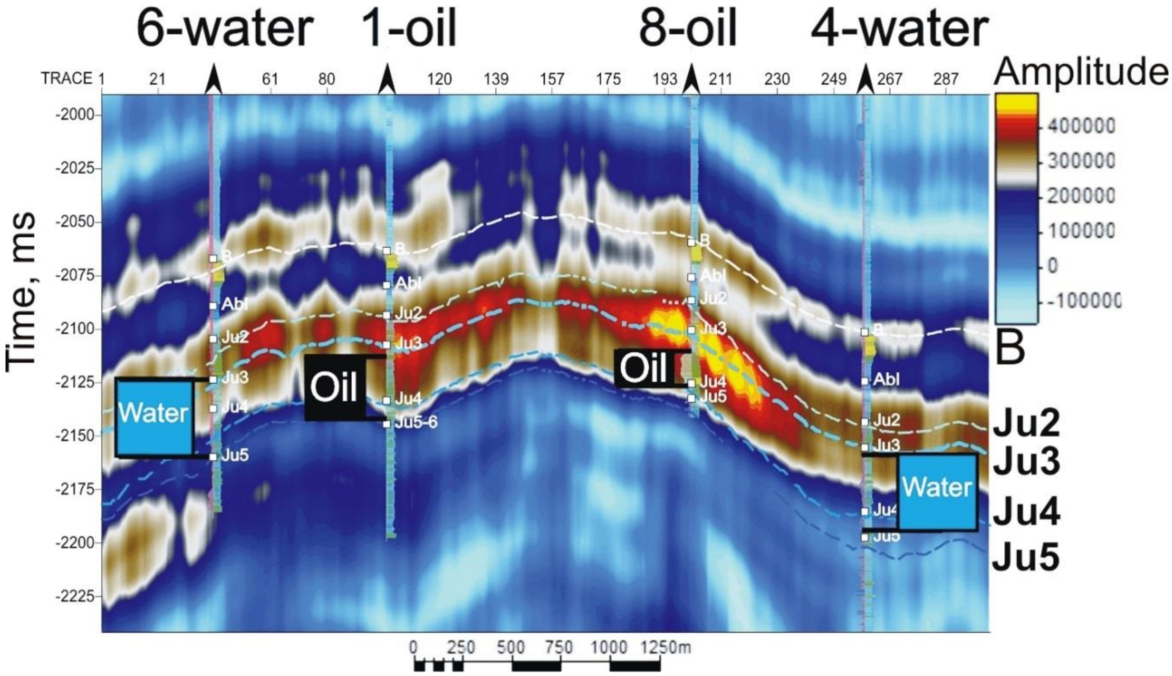

Figure 3.14 LF attribute at 10 Hz. High values of the LF attribute are connected with oil saturation zone.

CHAPTER FOUR

HYDROCARBON DETECTION

4.1 Low-frequency attribute

The results of the spectral decomposition substantiate the use of 10 Hz frequency seismic reflections. Moreover, the amplitude anomaly has been detected near the wells with oil. Therefore, it is necessary to apply the S transform to the whole seismic volume and calculate the LF attribute.

Figure 4.1 illustrates a map of this attribute in the form of the surface slice along the Ju_{3-4} formation. Based on the rules for the LF attribute calculation, it is expected that its high values on the map correspond to the zones of oil saturation and low values to the water saturation zones. It is possible to identify areas with anomalous values of the attribute on the map. High values of the LF attribute mostly correlate with the pure saturated oil wells over the territory. But this analysis does not take into account the thickness variation of the Ju_{3-4} reservoir. So it is sufficient to make the thickness compensation.

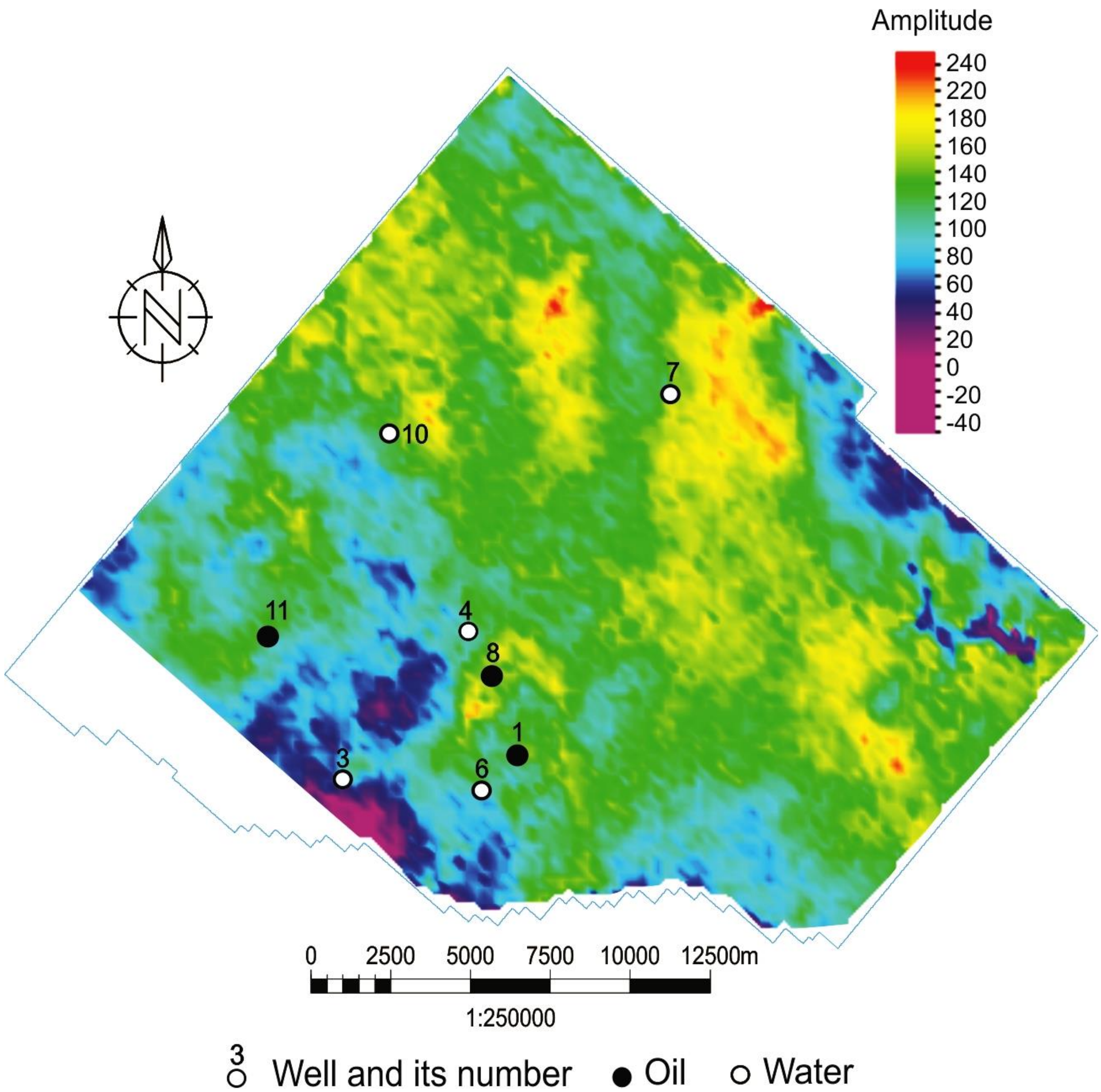

Figure 4.1 LF attribute horizon slice map for the $Ju_{3\text{-}4}$ formation. It shows that oil and water wells are located in high value and low value zones respectively.

4.2 Thickness compensation

Thickness compensation is a significant part of the amplitude analysis, as the thickness of the layer largely affects the seismic wave's amplitudes. Therefore, considering the influence of the thickness variations of the reservoir on the obtained results is essential in order to avoid an effect that could be interpreted as a hydrocarbon signature.

The LF attribute map of the $Ju_{3\text{-}4}$ formation in the form of the low frequency (10 Hz) is shown in Figure 4.1. High values on the map correspond to the zones of oil saturation and low values to the water saturation zones based on the attribute calculation. However, the fact that the thickness of the formation can cause similar anomalies necessitates the development of a useful approach for correcting this effect. As was mentioned before we have used the formula (3.3) for description of the P-wave reflection coefficient for a layer in case of normal incidence. The time thickness Δt_{xy} could be represented as the sum of $\Delta\bar{t}$, which is the average thickness of the layer in the area, and $\Delta\tilde{t}_{xy}$, which is the variable part of the full thickness:

$$\Delta t_{xy} = \overline{\Delta t} + \Delta\tilde{t}_{xy}, \quad (4.1)$$

$$\text{where } \Delta\bar{t} = \langle \Delta t_{xy} \rangle, \quad (4.2)$$

$$\text{and } \Delta\tilde{t}_{xy} = \Delta t_{xy} - \langle \Delta t_{xy} \rangle. \quad (4.3)$$

Hence, considering the model of the medium with R_i<<1 (i=1, 2) at a frequency of 10 Hz ($\omega\Delta\tilde{t}$, $\omega \to 2\pi 10$) at normal incidence we obtain an additive model of the reflection coefficient from a reservoir zone:

$$R \cong R_1 + R_2 e^{i\omega\bar{t}} + b\widetilde{t} \quad , \tag{4.4}$$

where b is a constant.

The obtained additive model was used for a correction of the amplitude values. The result is presented in Figure 4.2.The anomalies after correcting the thickness variation correlate with the pure oil wells better.

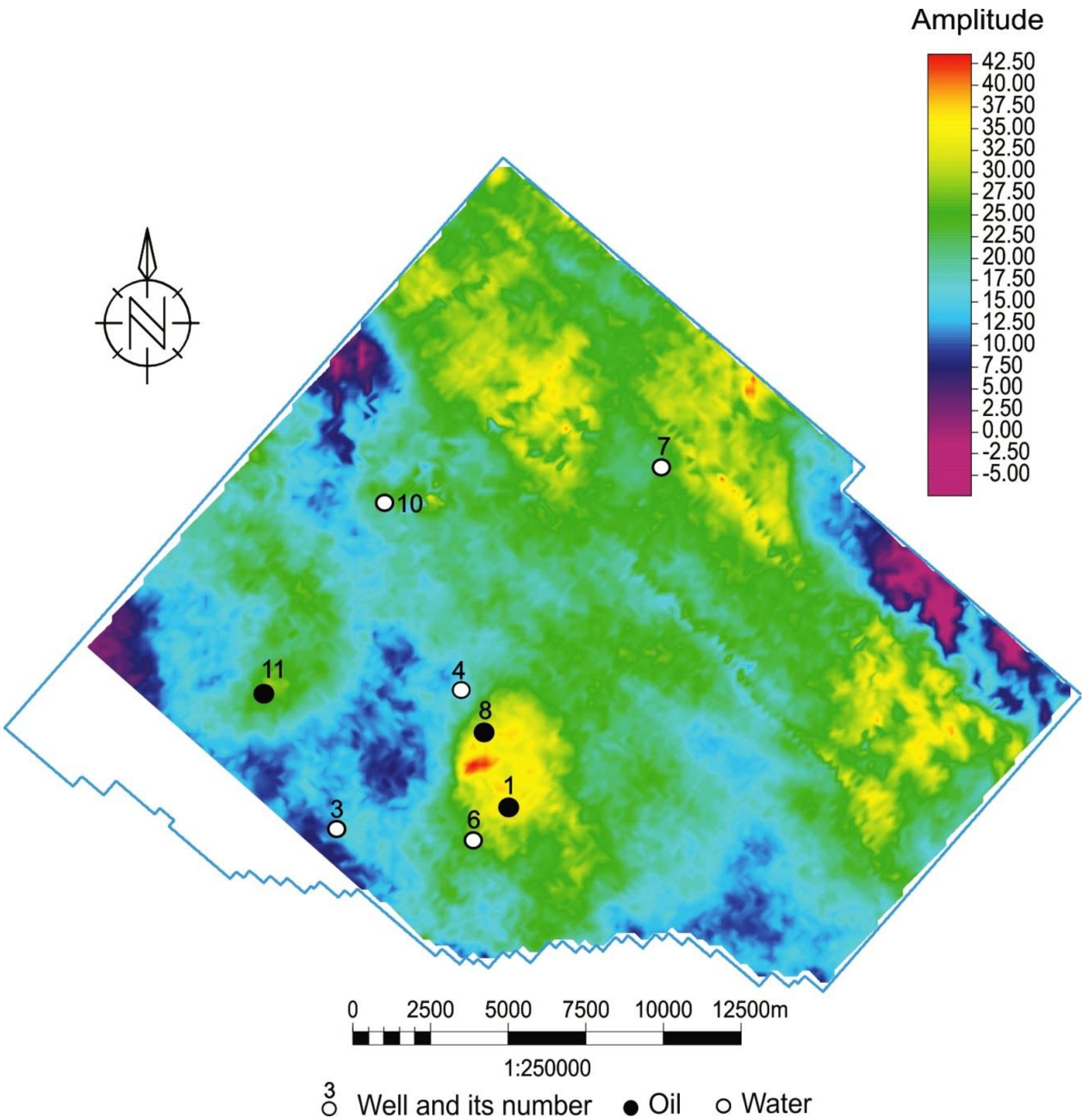

Figure 4.2 The Ju3-4 formation LF attribute map corrected for thickness. Oil and water wells are located in high value and low value zones respectively.

4.3 Quantitative analysis

The attribute for detecting oil-saturated zones within the Middle Jurassic Ju_{3-4} reservoirs in the cross-well space was obtained by using low-frequency amplitude analysis while taking into account the thickness variation of the reservoir. However, the LF attribute values are likely only able to distinguish between different types of fluid saturation qualitatively and approximately. At the same time, it is possible to make a quantitative analysis using the information of formation resistivity obtained from the resistivity log. It makes sense in order to separate relatively low-resistance water-saturated zones and high-resistance oil-saturated intervals, as increased resistivity of reservoirs is one of the main criteria for identification of oil-saturated zones, including the Ju_{3-4} formation.

The distribution of resistivity with pure saturation (only oil and only water) shows that there is a noticeable difference between water-saturated and oil-saturated wells (Figure 4.3). Moreover, it is possible to separate relatively low-resistance water-saturated zones and high-resistance oil-saturated intervals with a cutoff of 15-20 ohm-m within the analyzed area. In order to get a quantitative measure of the separation between the oil-saturated and water-saturated zones, it is necessary to convert the ST attribute to electrical resistivity through the correlation between them. The connection between electrical parameters and porous-visco-elastic properties of layers are rarely analytical and are instead usually correlation functions (Ljakhovitsky, 1989). This is due to the complexity and pluricausality of such links, especially when we are trying to establish a connection between the seismic attribute and electrical resistance.

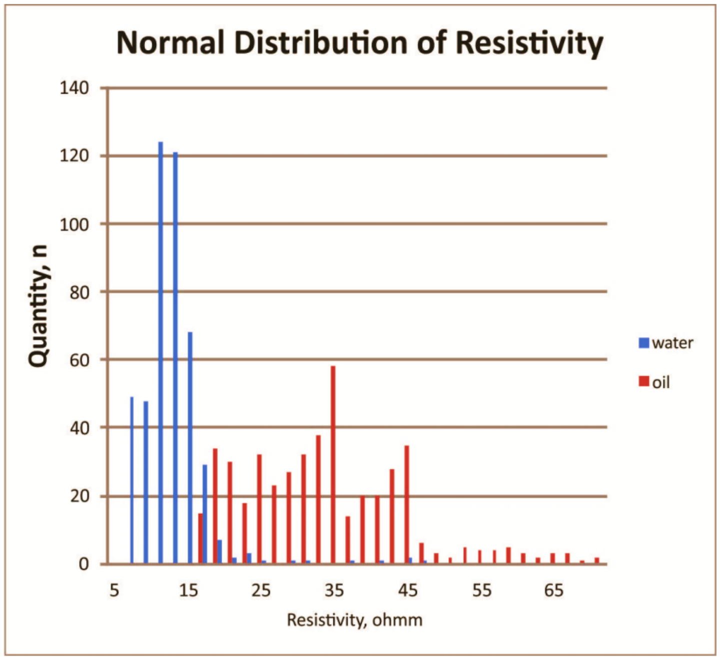

Figure 4.3 Normal distribution of Resistivity obtained from Resistivity log.

Figure 4.3 shows the correlation of the LF attribute values and resistance values; a sufficiently close relationship between them is noted. In accordance with the theory (Wiener, 1912) used, the mathematical expectation of resistivity was used as an effective resistivity of the reservoir's oil-saturated and water-saturated zones, measured in the wells with 10 cm intervals. To find the correlation between the LF attribute and resistivity eight wells were used. A selection of the wells was performed based on the single-phase fluid saturation in each well, resulting in three wells (1, 5, and 8) with pure oil and five wells (3, 4, 6, 7, and 10) with pure water. The wells are shown on the LF attribute map (Figure 4.2). The eight data points are not statistically valid enough for an absolutely reliable prediction of the saturation, but wells with mixed saturation (water with oil) would not help to get a better prediction of resistivity. To improve the prediction, we have assumed that zero resistivity corresponds to zero attribute value.

Based on the obtained correlation the LF attribute values were converted into the resistivity values. The resistivity map is presented in Figure 4.4. It contains all fifteen wells drilled in the study area. Seven of these wells were not involved in either selecting the scale (frequency) of the LF attribute or in obtaining the correlation between the attribute and resistivity. In general, there is a clear link between borehole information and the resistivity map. The resistivity anomalies (Figure 4.4) do not contradict the structural plan (Figure 2.9) on the majority of the map.

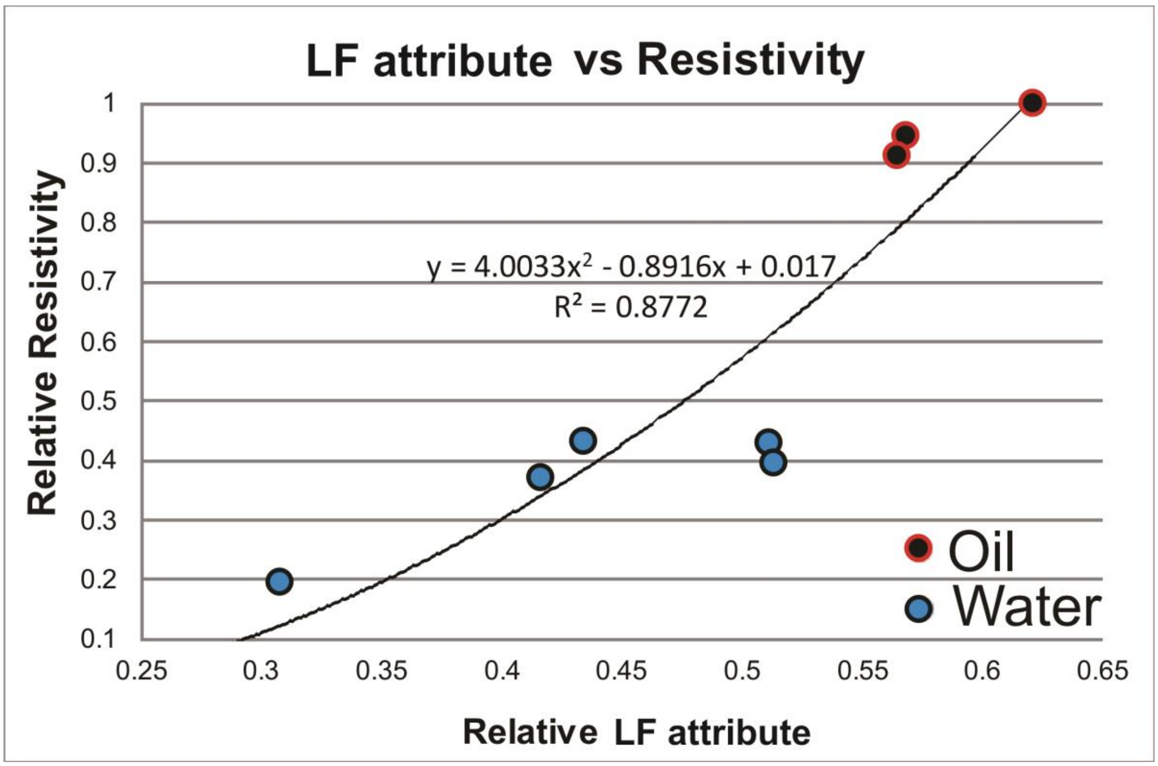

Figure 4.3 Correlation between Resistivity and LF attribute (R=0.93).

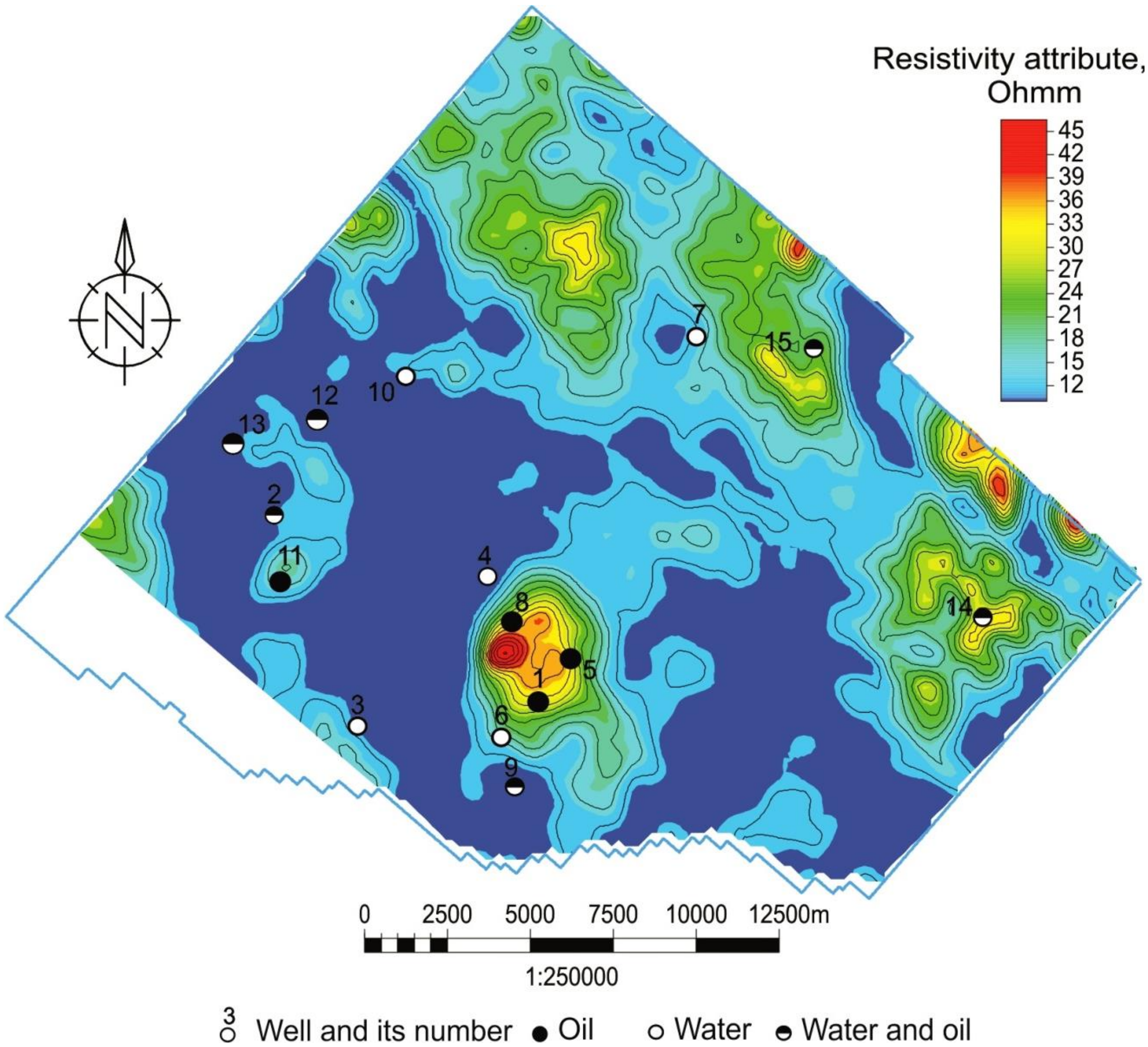

Figure 4.4 Resistivity attribute map of the $Ju_{3\text{-}4}$ formations with location of the wells. Map shows distribution of the high resistivity zones around wells with oil.

However, significant contradiction of the high-resistivity anomalies with the structural plan is seen between well 7 (water) and well 15 (oil and water). According to the forecast, a very high-resistivity anomaly implies an oil saturation of the Ju_{3-4} formation in this place. Such a prediction does not fit the scheme of the hydraulically connected wells 7 and 15. Figure 4.5 shows a fragment of the seismic section through wells 7 and 15. It indicates that most probably the wells are not connected hydraulically because the fault system (IL 4293-4277, XL 2004-2015) separates these wells. The vertical section of the LF attribute (Figure 4.6) over well 7 (water) and 15 (oil-water) clearly demonstrates a high LF attribute anomaly, which might be associated with the presence of oil.

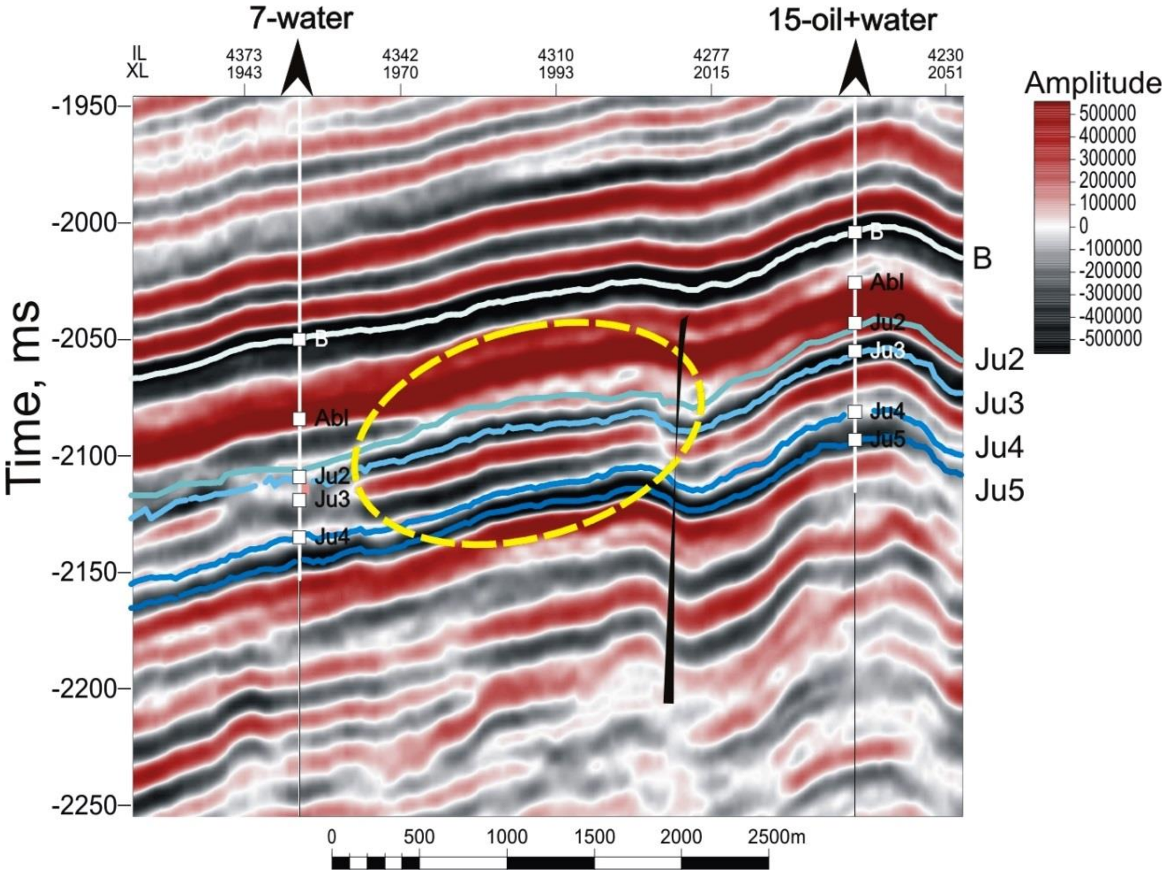

Figure 4.5 Full-stack seismic line over the well #7 (water) and well #15 (oil and water) shows that most probably the wells are not likely connected hydraulically, because the fault (IL 4293-4277, XL 2004-2015) separates these wells.

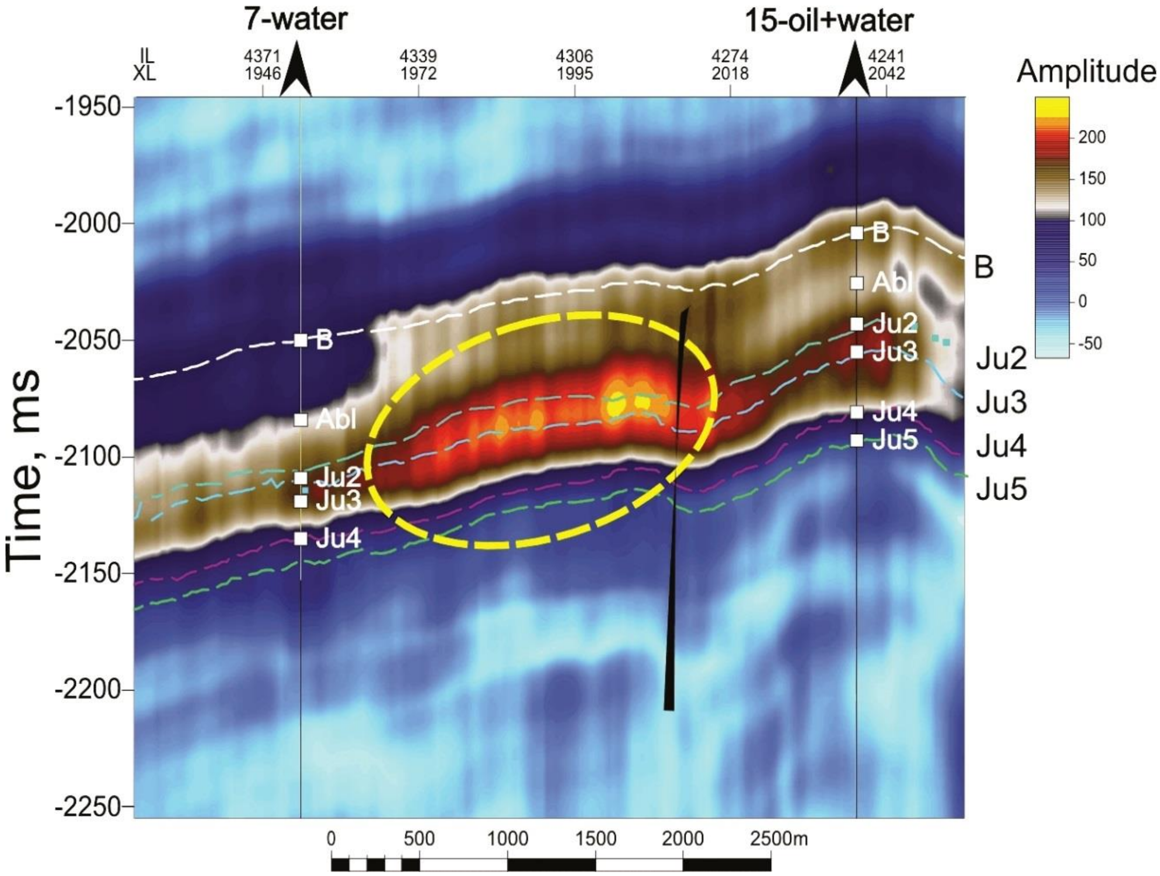

Figure 4.6 Vertical section of the LF attribute over the well #7 (water) and #15 (oil-water). The yellow dashed ellipse shows anomaly, which might be associated with the presence of oil.

CHAPTER FIVE

DISCUSSIONS AND CONCLUSION

5.1 Discussions

The obtained results showed that the use of the LF attribute with the support of information about formation resistivity as a quantitative criterion could work as a direct hydrocarbon indicator within the Middle Jurassic Ju_{3-4} formation. There are many examples when low-frequency anomalies were successfully used as an indication of hydrocarbons (Taner et al., 1979; Castagna et al., 2003), particularly in Western Siberia (Goloshubin et al., 2002, 2003, 2006). However, the mechanism generating these low-frequency anomalies is still not well understood.

Ebron, 1996, classified the possible mechanisms as stack-related and non-stack related. Stack-related mechanisms explain the low-frequency anomalies as uncertainties in the data processing, such as mis-stacking due to coarse velocity picking, locally converted shear waves, NMO stretch, etc. Nonstack-related mechanisms corresponds to reservoir attenuation, high-amplitude multiple reflections from top and bottom of the reservoir zone, deconvolution processing adding a low-frequency tail to the wavelet, etc. In the work of Tai et al., 2009, there is a classification of factors causing the low-frequency anomalies in two groups: global and local. On the one hand, global factors affect the whole seismic section (the source wavelet, the seismic data processing procedure, and the regional geologic structure); on the other hand, local factors affect seismic section locally due to lithological property changes, layer thickness variation, etc.

In addition to a variety of factors that can cause these anomalies, anomalies themselves separate into two types: low-frequency shadows, which are considerably delayed with respect to the thin reservoirs over them (Castagna et al., 2003), and low-frequency anomalies with no significant time delays in comparison with the reservoir reflections (Goloshubin et al., 2006). Accordingly, various mechanisms underlie these anomalies. Taking into consideration the anomalies with a significant time delay and assuming that the mechanism is nonstack-related and local, it is possible to explain them by an anomalous amount of mode conversions between fast and slow P-waves (Chabyshova et al., 2014).

In the case of the Ju_{3-4} reservoir we have seen a slight time delay of low-frequency anomalies in comparison with the reservoir reflections. Numerous laboratory and field experiments showed that such anomalies could be associated with the frequency attenuation and velocity dispersion (Gurevich et al., 1997, Rapoport et al., 2004). Korneev et al., 2004, presented the results of detailed study of the low-frequency anomalies phenomena that could be explained by diffusive-viscous attenuation. Low-frequency anomalies associated with the hydrocarbon saturation of the reservoirs in West Siberia are exactly explained by this mechanism (Goloshubin et al., 2006), particularly within the Jurassic deposits in the southern part of Western Siberia (Goloshubin et al., 2003). Therefore, based on the previous studies, it is possible to make a hypothesis that the oil saturation can cause low-frequency anomalies within the Ju_{3-4} reservoirs due to attenuation and velocity dispersion. However, more precise study is needed.

5.1 Conclusion

The Middle Jurassic sandstone reservoir $Ju_{3\text{-}4}$ has a discrete distribution and a complex irregular shape according to the well and seismic information within the study area. A tectonic and stratigraphic overview indicates that the area is situated in a complex lithological and stratigraphic environment. Therefore, the structural factor is not determinative for identification of the hydrocarbon deposits within the $Ju_{3\text{-}4}$ formation. The detection of the hydrocarbons is also complicated due to the presence of the strong reflected wave from the Bazhenovskaya (B) formation above the zone of interest.

In order to solve this problem amplitude analysis versus offset (AVO) and frequency-dependent (FD) amplitude analysis was applied. The results of modelling and testing on the real data showed that AVO does not work throughout the area because of the low effect of fluid compressibility on the mature and consolidated sandstones of the $Ju_{3\text{-}4}$ formation as well as interference of the reflection wave from $Ju_{3\text{-}4}$ with the wave from horizon B. However the FD analysis produced satisfactory results. At low frequencies the effect of the strong reflected wave of the B formation is almost suppressed. Low-frequency amplitude anomalies were detected near the oil wells. The LF attribute was developed based on the results.

The LF attribute was used for direct hydrocarbon detection. The LF attribute compensation due to thickness variation of the reservoir was made. The additive model of the seismic reservoir response, including the thickness variations, was developed and applied. The nature of the low-frequency amplitude anomaly was connected with the hypothesis that the oil saturation within reservoirs can cause frequency attenuation and velocity dispersion. Based on the LF attribute results it is possible to qualitatively separate oil-saturated zones from water-saturated zones. In order to make a quantitative separation, the formation resistivity was used. The resulting map of the relative formation resistivity was presented. It shows sufficient correlation with the information obtained from well drilling and interpretation of well logging data.

The principal possibility of the detection and mapping of oil-saturated zones within the Middle Jurassic reservoirs in the cross-well space was shown. It is based on the low-frequency amplitude analysis of seismic data and use of the information from the log data and well testing. It takes into account the thickness variation of the reservoir and includes the quantitative criterion for the separation of oil-saturated zones from water-saturated zones within the study area.

REFERENCES

Bochkarev , V.S., 1977, The structure of the basement of the West Siberian plate and some general questions of tectonics of the platform regions: Trudy ZapSibNIGNI, **125**

Boganic, G.N. and I.I. Gurvich, 2006, Seismic exploration: Tver.

Brekhovskikh, L.M., 1980, Waves in Layered Media, Second Edition: Academic Press Inc.

Castagna, J. P., and Swan, H.W., 1997, Principles of AVO crossplotting: The Leading Edge, **17**, 337–342.

Castagna, J. P., S. Sun, and R. W. Siegfried, (2003), Instantaneous spectral analysis: Detection of low-frequency shadows associated with hydrocarbons: The Leading Edge, **22**, 120–127.

Chakraborty, A and D. Okaya, 1995, Frequency-time decomposition of seismic data using wavelet-based methods: Geophysics, **60**, 1906-1916.

Chabyshova,E. and G.Goloshubin, 2014, Seismic modeling of low-frequency "shadows" beneath gas reservoirs: Geophysics, **79**, 417-423.

Cohen, L., 1995, Time-Frequency Analysis: Prentice-Hall Inc., Signal Processing Series.

Ebrom, D., (2004), The low frequency shadow on seismic sections, The leading Edge, **23**, 772

Goloshubin, G. M., and Korneev, V. A., 2000. Seismic low-frequency effects from fluid- saturated reservoir. SEG Technical Program Expanded Abstracts, **19**, 1671-1674.

Goloshubin, G. M., V. A. Korneev, and V. M. Vingalov, 2002, Seismic low-frequency effects from oil-saturated reservoir zones. SEG Technical Program Expanded Abstracts, 1813-1816.

Goloshubin, G. M., V. M. Vingalov, Ju. A. Stovbun, O. V. Bakuev, M. G. Latfullin, 2003, Technology of oil-saturated zones prognosis based on seismic data: Application to south of Tyumen region: Geophysics, Special issue "Seismic Technologies – 2", 70-74.

Goloshubin, G., C. VanSchuyver, V. Korneev, D. Silin, and V. Vingalov, 2006, Reservoir imaging using low frequencies of seismic reflections, The Leading Edge, **25**, 5, 527-531.

Gurary, F. G., V. P. Devjatov, V. I. Demin, et al., 2005, Geological structure and petroleum potential of low - middle Jurassic in West-Siberian province, "*Nauka*", 156 p.

Gurevich, B., V. B. Zyrianov, and S. L. Lopatnikov, 1997, Short note: Seismic attenuation in finely layered porous rocks: Effects of fluid flow and scattering: Geophysics,62, 319–324.

Hilterman, F. J., 2001, Seismic Amplitude Interpretation, SEG/EAGE, Distinguished Instructor Series, No 4.

Korneev, V., G. Goloshubin, T. Daley and D. Silin, 2004, Seismic low-frequency effects in monitoring of fluid-saturated reservoirs: Geophysics, **69**, 2, 522-532.

Ljakhovitsky, F. M., V. K. Khmelevskoy, Z. G. Jashenko, 1989, Engineering geophysics, “Nedra”, 252 .

Rapoport, M. B., L. I. Rapoport, and V. I. Ryjkov, 2004, Direct detection of oil and gas fields based on seismic inelasticity effect: The Leading Edge, **23**, 276–278.

Ren, H., G. Goloshubin, and F. Hilterman, 2007, Spectra Crossplot: The Leading Edge, **26**, 12, 1562-1566

Rutherford, S.R. and R.H. Williams, 1989, Amplitude-versus-offset variations in gas sands: Geophysics, **54,** 6, 680-688.

Shimansky, V.V., S. F. Khafizov, N. B. Taninskaja, R. T., Eganjanc, N. N. Kolpenskaja, T. D. Shibina, 2004, Sedimentation models of Jurassic formations in South of Tyumen region as a basis of the forecast of petroleum potential, Oil lithology, Nonstructural traps and nontraditional types of reservoirs, “Nedra”, 50-61.

Simm R. and M.Bacon, 2014, Seismic Amplitude: An Interpreter’s handbook: Cambridge University Press

Smith, G.C., and Gidlow, P.M., 1987, Weighted stacking for rock property estimation and detection of gas: Geophysical Prospecting, **35**, 993-1014.

Stockwell, R. G., L. Mansinha, and R. P. Lowe, 1996, Localization of the complex spectrum-the *S* Transform: IEEE Transactions on Signal Processing, **44**, 4, 998-1001.

Tai, S., Puryear, C., and Castagna, J. P., 2009. Local frequency as a direct hydrocarbon indicator. SEG Technical Program Expanded Abstracts, 28, 2160-2164.

Taner, M. T., F. Koehler, and E. Sheriff, 1979, Complex seismic trace analysis: Geophysics, **44**, 1041–1063.

Wiener O. Die Theorie des Mischkörpers für das Feld der stationären Strömung, Abhandl. Math.-phys. Kl. Köngl. Sächs. Ges. Wiss. 1912. Vol. 32. P. 507–604.

Ulmishek G.F.,2003, Petroleum Geology and Resources of the West Siberian Basin, Russia, U.S.Geological Survey Bulletin 2201-G